

# Ore Genesis for Stratiform Ore Bodies of the Dongfengnanshan Copper Polymetallic Deposit in Yanbian Area, NE China: Constrains from LA-ICP-MS in situ Trace Elements and Sulfide S-Pb Isotopes

LU Siyu<sup>1</sup>, REN Yunsheng<sup>1,2,\*</sup>, YANG Qun<sup>1</sup>, SUN Zhenming<sup>1</sup>, HAO Yujie<sup>1,3</sup> and SUN Xinhao<sup>1</sup>

<sup>1</sup> College of Earth Sciences, Jilin University, Changchun, 130061, China

<sup>2</sup> Institute of Disaster Prevention, Beijing, 101601, China

<sup>3</sup> Key Laboratory of Mineral Resources Evaluation in Northeast Asia, Ministry of Natural Resources of China, Changchun, 130061, China

**Abstract:** The Dongfengnanshan Cu polymetallic deposit is one representative deposits of the Tianbaoshan ore district in Yanbian area, northeast (NE) China. There occur two types of ore bodies in this deposit, the stratiform ore bodies and vein-type ones, controlled by the Early Permian strata and the Late Hercynian diorite intrusion, respectively. Due to the ambiguous genetic type of the stratiform ore bodies, there has been controversy on the relationship between them and vein-type ore bodies. To determine the genetic type of stratiform ore bodies, laser ablation inductively coupled plasma mass spectrometry (LA-ICP-MS) in situ trace elements and S-Pb isotope analysis have been carried on the sulfides in the stratiform ore bodies. Compared with that in skarn, Mississippi Valley-type (MVT), and epithermal deposits, sphalerite samples in the stratiform ore bodies of the Dongfengnanshan deposit are significantly enriched in Fe, Mn, and In, while depleted in Ga, Ge, and Cd, which is similar to the sphalerite in volcanic-associated massive sulfide (VMS) deposits. Co/Ni ratio of pyrrhotites in the stratiform ore bodies is similar to that in VMS-type deposits. The concentrations of Zn and Cd of chalcopyrites are similar to those of recrystallized VMS-type deposits. These characteristics also reflect the intermediate ore-forming temperature of the stratiform ore bodies in this deposit. Sulfur isotope compositions of sulfides are similar to those of VMS-type deposits, reflecting that sulfur originated from the Permian Miaoling Formation. Lead isotope compositions indicate mixed-source for lead. Moreover, the comparison of the Dongfengnanshan stratiform ore bodies with some VMS-type deposits in China and abroad, on the trace elements and S-Pb isotope characteristics of the sulfides reveals that the stratiform ore bodies of the Dongfengnanshan deposit belong to the VMS-type, and have closely genetic relationship with the early Permian marine volcanic sedimentary rocks.

**Key words:** LA-ICP-MS in situ trace element; S-Pb isotope; VMS-type; stratiform ore bodies; Dongfengnanshan copper polymetallic deposit; Tianbaoshan ore district

E-mail: renys@jlu.edu.cn

## 1 Introduction

The Yanbian area, located in the eastern segment of the Central Asian Orogenic Belt (CAOB) (Fig. 1a), is an important metallogenic province in NE China, and hosts large amounts of copper, gold, tungsten, lead, zinc and molybdenum deposits. The Tianbaoshan ore district in the central-eastern part of the Yanbian area has been mined for more than 100 years. More than 10 polymetallic deposits (mineral occurrences) such as Lishan (Pb-Zn), Xinxing (Ag-Pb-Zn), Dongfengbeishan (Mo) and Dongfengnanshan (Cu-Pb-Zn) have been discovered in this district. In the former three deposits, systematic isotope and fluid inclusion studies have been carried out to document the ore genesis, tectonic settings and sources of ore-forming materials (Chen, 2009; Ju, 2013; Zhang et al., 2011, 2012, 2013a, b; Sun et al., 2014; Yang et al., 2015b, 2018; Wang et al., 2017a). However, due to less exploration and research, the ore genesis of the Dongfengnanshan deposit remains unclear. For the two types of ore bodies, stratiform and vein-type in the deposit, some researchers believe that they both resulted from the same mineralization event in different ore-hosting spaces, either the Late Paleozoic VMS-type (Liu et al., 2000) or Mesozoic contact metasomatic type (Zhang et al., 2011, 2012, 2013a, b). Another view suggested that stratiform ore bodies were formed in the Permian submarine volcanic eruptions, and original stratiform ore source layers had been overprinted by the Late Hercynian magmatism (Li et al., 1991). Recently, Ren et al. (2015) supposed that mineralized age of stratiform ore bodies should be Early Permian, while vein-type and skarn ore bodies were transformed by the subsequent ore-bearing magmatic hydrothermal fluid. The key point of the divergences is the genesis of stratiform ore bodies.

This article has been accepted for publication and undergone full peer review but has not been through the copyediting, typesetting, pagination and proofreading process, which may lead to differences between this version and the [Version of Record](#). Please cite this article as [doi: 10.1111/1755-6724.14358](https://doi.org/10.1111/1755-6724.14358).

This article is protected by copyright. All rights reserved.

In situ LA–ICP–MS analysis is an efficient method to determine trace elements of diverse sulfides (Watling et al., 1995; Cook et al., 2009) and comparable compounds (Ciobanu et al., 2009), and is significant in determining the origin of the sulfides. To determine the genesis of stratiform ore bodies in the Dongfengnanshan deposit, LA–ICP–MS analyses have been conducted on sulfides from the stratiform ores for trace elements concentration. Moreover, S–Pb isotopes of sulfides selected from stratiform ores have also been analyzed to determine the source of the ore-forming materials. With comparison of trace elements composition of sulfides to which from different types polymetallic deposits, the ore genesis of stratiform ore bodies in the Dongfengnanshan has been discussed.

## 2 Geological Settings

### 2.1 Tectonic Setting

As one of the largest accretionary orogens in the world (Sengör et al., 1993; Khain et al., 2002; Windley et al., 2007), the CAOB extends from the European Craton to the Pacific Ocean and separates the North China from the Siberia Plate. In NE China, the CAOB can be divided into five blocks, including the Erguna, Xing'an, Songnen, Jiamusi and Khanka Massif from west to east (Fig.1b) (Sengör et al., 1993; Jahn et al., 2000; Wu et al., 2007, 2011; Cao et al., 2012, 2013; Chai et al., 2016a, b, c). The Yanbian area is located in the Songnen block. Since the Paleozoic period, this region has been controlled by the subduction and closure of the Paleo-Asian Ocean and subduction of the Paleo-Pacific Plate, which resulted in intensive tectono-magmatic activities and favorable geological setting for endogenous metal mineralization (Wu et al., 2007, 2011; Xu et al., 2013; Chai et al., 2015; Wang et al., 2016; Zhao, 2018; Chen et al., 2019), including the Late Paleozoic and Mesozoic strata, E–W, S–N, NE–NNE and NW faults, as well as Hercynian, Indosinian and Yanshanian magmatisms (Fig.1c).

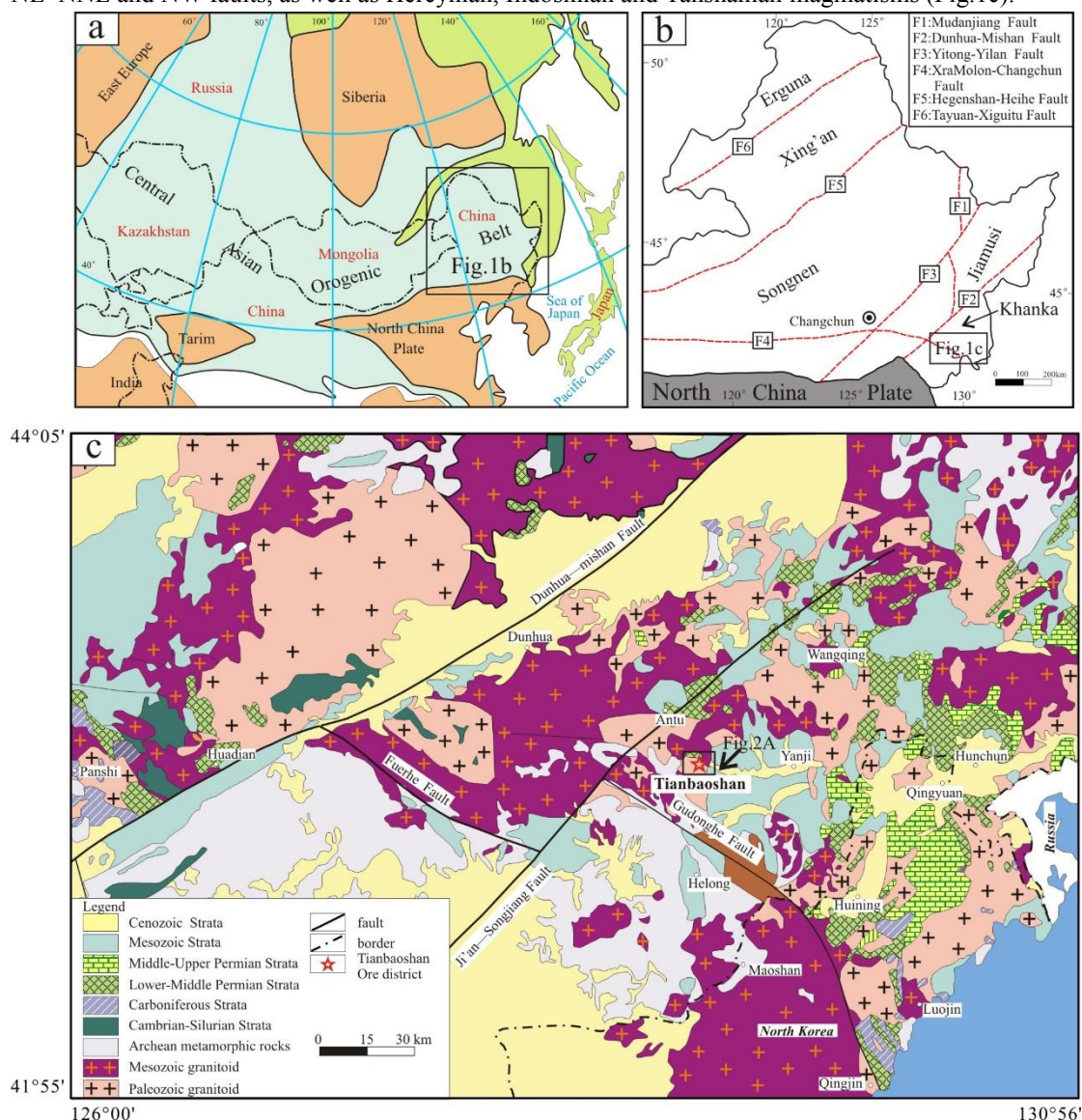


Fig. 1. (a) Location of the Central Asian Orogenic Belt (modified from Jahn et al., 2000); (b) Geologic map of NE China (modified from Wu et al., 2011); (c) Simplified regional geological map of the Yanbian area (modified from Shang et al., 2017).

## 2.2 Ore District Geology

The Tianbaoshan ore district lies in the eastern part of the Yanbian area, the strata in the ore district mainly include the Early Carboniferous Shanxiuling Formation ( $C_{1s}$ ), the Early Permian Miaoling Formation ( $P_{1m}$ ), the Late Permian Qinglongcun Group ( $P_{2q}$ ) and the Middle Jurassic Mingyuegou Formation ( $J_2m$ ) (Fig.2a). The Shanxiuling Formation is composed mainly of marine carbonates with clastic rocks intercalations including marble, crystalline limestone with micacite intercalations, and phyllite. The Miaoling Formation is a set of marine volcanic sedimentary rock system composed of carbonates and flyschoid formations. The lower member of the Miaoling Formation consists of intermediate–acid volcanic rocks such as andesite, andesitic conglomerate and rhyolite; the middle member includes mainly interbedded carbonate rocks with andesitic tuff–dacite; and the upper member is composed of volcanic rocks such as andesite and andesitic tuff. The Qinglongcun Group is characterized by the low–level metamorphic epizonal metamorphic rocks such as amphibolite, felsic schist, andalusite–quartz schist and biotite–plagioclase schist. The Mingyuegou Formation is a continental volcanic sedimentary rock series composed of andesite and glutenite.

The NE–, NW–trending faults and their secondary fractures were widely developed in the ore district. Among them, the NE–trending faults are the earliest, and controlled the distribution of Paleozoic strata and magmatic rocks. The NW–trending faults cut the NE–trending faults and provided migration tunnels, metallogenic power, and ore–hosting space for afterward hydrothermal ore bodies.

According to previous geological and isotope dating data (Ju, 2013; Sun et al., 2014; Yang et al., 2015b, 2018), four–periods of magmatic intrusions in the ore district has been clarified: (1) the Late Hercynian granodiorites and diorites (285–255Ma), distributed mainly in the eastern and central parts of the ore district, and intruded in the Shanxiuling Formation; (2) the Indosinian granitoids (249–205Ma), occur in the southern part of the ore district; (3) the Early Yanshanian granitic rocks (198–153Ma); (4) the Late Yanshanian diorite porphyries (129–105Ma).

Due to favorable geological settings and ore–forming conditions, multiple mineral resources and mineralization types formed in the Tianbaoshan ore district. Typical deposits include the Lishan skarn (Pb–Zn) deposit, the Xinxing cryptoexplosive breccia–type (Ag–Pb–Zn) deposit, the Dongfengbeishan porphyry (Mo) deposit and the Dongfengnanshan (Cu–Pb–Zn) deposit.

## 2.3 Deposit Geology

The Dongfengnanshan copper polymetallic deposit lies in the eastern part of the Tianbaoshan ore district. There develop the stratiform and veined ore bodies, which are hosted by the volcanic sedimentary rocks of the Early Permian Miaoling Formation and the Late Hercynian diorite, respectively (Fig.2b).

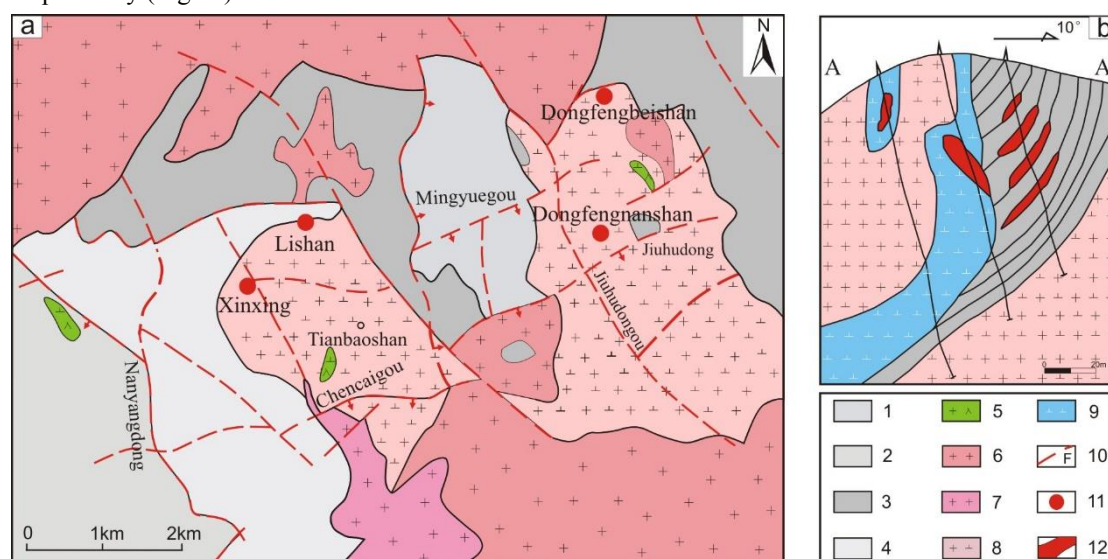


Fig. 2. (a) Geological map of the Tianbaoshan ore district (modified from Wang et al., 2017a; Yang et al., 2018); (b) NO.5 Geological section line map of the Dongfengnanshan deposit (modified from Ju, 2013).

1, Middle Jurassic Mingyuegou Formation; 2, Upper Permian Qinglongcun Group; 3, Lower Permian Miaoling Formation; 4, Lower Carboniferous Shanxiuling Formation; 5, Late Yanshanian diorite porphyrite; 6, Early Yanshanian granitoid; 7, Indosinian granitoid; 8, Late Hercynian granodiorite; 9, Late Hercynian diorite; 10, fault; 11, ore deposit; 12, ore bodies.

The stratiform ore bodies are hosted in the intermediate–acidic volcanic rocks and limestone of the Miaoling Formation, and concordant with the surrounding rocks. They extend tens to hundreds meters in length, several to tens of meters in thickness with dip angle from 30 to 60°. The ore bodies are hosted in special volcanic sedimentary exhalative metamorphic rocks formerly known as hornfels and/or mylonite (Sun, 1994; Chen, 2009). The host rocks are characterized by Zn–rich spinel, existing cordierite hornfels and barite lamellae (Sun, 1994) that formed under high–temperature and high–pressure conditions during the eruption of submarine volcanoes. Ore structures include mainly banded (Fig.3a) and disseminated, and the ore textures are mainly anhedral–granular and weakly metasomatic (Figs.3b, 3c). Weak wall–rock alterations include silicification, chloritization and epidotization (Figs.3d, 3f). Major metal minerals include chalcopyrite, sphalerite, pyrrhotite, pyrite, galena and arsenopyrite, while non–metal minerals include quartz, chlorite, and fluorite.

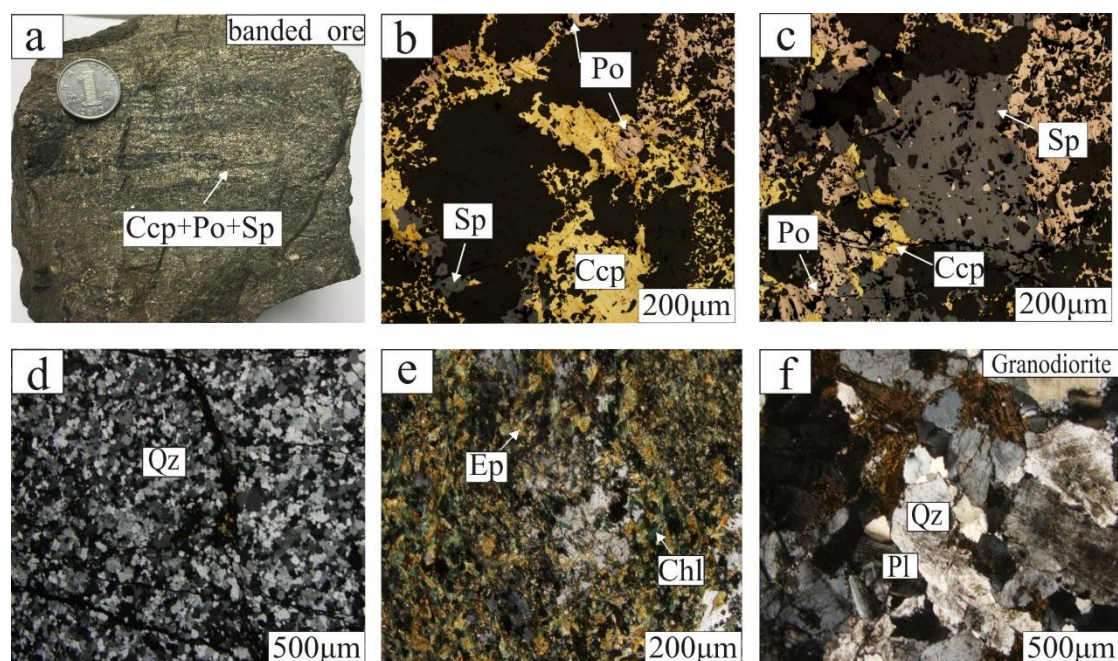


Fig. 3. Mineral compositions, ore textures, ore structures, altered granodiorite and unaltered granodiorite. (a) Banded ore; (b) Anhedral granular texture in the stratiform ore; (c) Pyrrhotite replaced weakly by chalcopyrite in the stratiform ore and the clear boundary between sphalerite and pyrrhotite; (d) Silicification in the wall rocks; (e) Chloritization and epidotization overprinted on the wall rocks; (f) Granodiorite. Ccp–chalcopyrite; Sp–sphalerite; Po–pyrrhotite; Ep–epidote; Chl–chlorite; Qz–quartz; Pl–plagioclase.

The vein–type ore bodies occur near the contact zone of diorite and carbonate rocks, and obviously controlled by near EW–trending structural fractures, cutting earlier stratiform ore bodies and their ore–bearing surrounding rocks. They extend several to tens of meters in length, several meters in thickness with dip angle from 45 to 70°. Ore structures consist of massive and network structure and ore textures dominantly include metasomatic texture. Such wall–rock alterations develop as epidotization, chloritization, skarnization and carbonation. Major metal minerals include chalcopyrite, sphalerite, pyrrhotite, pyrite, galena and magnetite. Besides calcite and quartz, gangue minerals also include such skarn minerals as garnet.

### 3 Samples and Methods

The samples were collected from the open pits of the Dongfengnanshan mine district (42°56'55"N, 124°30'30"E) for LA–ICP–MS in situ trace elements and S–Pb isotope analysis. The ore samples collected are grey–black with banded structures (Fig.3a), and the metal minerals were mainly sphalerite (25%), pyrrhotite (40%), and chalcopyrite (20%).

In situ trace element analyses were conducted by LA–ICP–MS at the State Key Laboratory of Ore Deposit Geochemistry, Institute of Geochemistry, Chinese Academy of Sciences (IGCAS). Laser sampling was performed by using an ASI Resolution–LR–S155 laser microprobe equipped with a Coherent Compex–Pro 193 nm ArF excimer laser. An Agilent 7700x ICP–MS instrument was used to acquire the ion–signal intensities. The He was applied as a carrier gas at a speed of 350 mL/min. The ablated aerosol was mixed with Ar (900 mL/min) as a transport gas before exiting the cell. Each analysis incorporated a background acquisition of approximately 30 s (gas blank) followed by 60 s of data acquisition from the sample. Analyses were run with 26 µm pit size, 5 Hz pulse frequency, and 3J/

cm<sup>2</sup> fluence.

The internal standard Pyrite was used for calibrating the concentrations of S and Fe. The integrated count data for concentrations of other elements were calibrated and converted by using United States Geological Survey (USGS) GSE-1G and GSD-1G reference glasses. The preferred values of the element concentrations for these reference glasses were taken from the GeoReM database. Sulfide reference material MASS-1 was analyzed as unknown sample to verify the analytical accuracy.

The S-Pb isotope analyses were completed at the Research Institute of Uranium Geology, Beijing. The sulfides were pulverized to 200 mesh before the test and were selected to have >95% purity. In the S isotope composition analysis, the sulfides and Cu<sub>2</sub>O were heated under a vacuum to form SO<sub>2</sub>, which was then analyzed by using a Delta V Plus gas isotope MS instrument. The δ<sup>34</sup>S values were based in the Vienna standard troilite in Canyon Diablo meteorite (V-CDT) standard, and the test accuracy was about ±0.2‰. For the Pb isotope ratio analysis, the sulfide samples were first leached with hot acid and were then tested on an Isoprobe-T hot surface ionization MS instrument using the standard sample NBS981. The Pb isotope test values were <sup>208</sup>Pb/<sup>206</sup>Pb = 2.1681 ± 0.0008, <sup>207</sup>Pb/<sup>206</sup>Pb = 0.91464 ± 0.00033, <sup>204</sup>Pb/<sup>206</sup>Pb = 0.059042 ± 0.000037, and the test accuracy was >0.08%.

## 4 Results

### 4.1 In Situ LA-ICP-MS Trace Element of Sulfides

For the sphalerite, pyrrhotite and chalcopyrite in the ore of the stratiform ore bodies of the Dongfengnanshan deposit, 25 spots were analyzed, respectively. The results and related parameters of the elements are shown in Tables 1, 2 and 3. The ranges in absolute concentrations for the selected elements are shown as histograms in Figs. 4, 5 and 6.

The ω(Fe) of the sphalerite varies from 11.2wt% to 18.8wt%, with an average content of 12.3wt%, which indicate the analyzed sphalerite belonging to Fe-sphalerite (Table.1). This concentration is significantly higher than that of the sphalerite in skarn deposits (e.g., Oca de Fier) and MVT deposits (e.g., Niujiaotang) and is similar to which in VMS-type deposits (e.g., Laochang, 12.2 wt%–15.4 wt%, Ye et al., 2012). Except for one spot at 6318 ppm, the concentrations of Mn are 1433–2085 ppm, which are less variable and similar to which in VMS-type deposits (e.g., Bainiuchang) and skarn deposits (e.g., Hetaoping), and higher than those of the sphalerite in other types of deposits. The concentration of In range from 394 to 643 ppm with an average concentration of 496 ppm, which is several to several hundred times higher than those of the sphalerite in other types of deposits but is similar to that of the sphalerite in VMS-type deposits such as Laochang, with a mean concentration of 200 ppm (Ye et al., 2012). The ω(Cd), varied from 4372 to 5808 ppm, is lower than which in epithermal deposits (e.g., Toroiaga Tga-1), near to which in VMS-type deposits such as Vorta DMV, with a mean concentration of 4744 ppm (Cook et al., 2009), and skarn type deposits such as Hetaoping, with a mean concentration of 4737 ppm (Ye et al., 2011). The ω(Ga) varies from 0.12 to 0.7 ppm, which is less than that in the MVT deposits (e.g., Mengxing). The ω(Ge) varies from 1.9 to 5.8 ppm, which is lower than that in the epithermal deposits (e.g., Rosia Montana). The Co concentration varies from 105 to 158 ppm with an average of 126 ppm, which is similar to that in skarn deposits such as Hetaoping, with a mean of 212 ppm, and Luziyuan, with a mean of 323.8 ppm (Ye et al., 2011). The ω(Sn) is between 0.76 and 29.31 ppm and the ω(Sb) is between 0.2 and 2.97 ppm (Fig.4). The Cu, Pb, and Bi concentrations are 323.9–901.3 ppm, 1.94–22.09 ppm, and 0.51–6.68 ppm, respectively, and with obvious varieties. The Se has a spot concentration lower than the minimum detection limit, and the rest ranged from 4.56 to 12.79 ppm with an average concentration of 9.05 ppm.

The ω(Co) and ω(Ni) of the pyrrhotite vary at 128.81–192.25 ppm and 47.58–270.86 ppm, respectively. Co is more stable than Ni, and Co/Ni is 0.63–3.11 (Table.2), similar to which in massive sulfide deposits, such as Dabaoshan, with a mean of 2.20 (Liu et al., 2019), and is higher than which in Cu-Ni sulfide deposits (e.g. Creighton) and skarn deposits (e.g., Hongshan). The contents of Cu, Zn, Ag, Se, Sb, Pb, and Bi vary widely (Fig.5). Among them, Cu, Zn, Ag, and Pb show a wide range of variation at 0.86–13.24 ppm, 0.85–68.4 ppm, 0.61–10.8ppm, and 0.73–30.21 ppm, respectively. The concentrations of the Se, Sb, and Bi vary at 5.79–17.05 ppm, 0.05–0.59 ppm, and 0.24–4.53 ppm, respectively. Among the seven elements, Sb is depleted, and the other six are relatively enriched. Ge is stable with a concentration of 10.83–17.3 ppm and an average of 12.74 ppm.

The Co concentration of the chalcopyrite varies from 0.91 to 8.54 ppm, with an average of 3.82 ppm. The Ni concentration of over half of the spots is lower than the minimum detection limit, and the concentration of other spots varies from 0.89 to 3 ppm. Co and Ni concentrations are lower than those of the chalcopyrite in the Cu-Ni sulfide deposits such as Jinchuan, similar to those in VMS-type deposits such as Vorta, with a mean Co concentration of 1.5 ppm; Ni concentration is below the minimum detection limit (George et al., 2018; Table.3, 4). The variation in Zn and Cd concentration is moderate, at respective ranges of 293–720 ppm and 6.29–14.79 ppm and means of 514 ppm and 9.31 ppm. Zn concentration is slightly less than epithermal deposits (e.g., Herja) and skarn deposits (e.g., Baita Bihor), higher than which in porphyry deposits (e.g., Bor), and similar to which in recrystallized

**Table 1 In situ LA-ICP-MS trace element contents in the sphalerite in Dongfengnanshan deposit (ppm)**

	Mn55	Fe57 (wt%)	Co59	Ni60	Cu65	Ga71	Ge72	Se77	Ag107	Cd111	In115	Sn118	Sb121	Pb208	Bi209
TB-6-1	1874	12.23	144.4	–	526.1	0.200	2.770	11.69	12.61	5065	576.2	3.920	0.960	7.530	2.310
TB-6-2	2559	12.91	142.7	1.670	510.3	0.290	3.210	6.290	10.71	4794	558.8	29.31	1.030	10.50	2.150
TB-6-3	2185	11.84	124.3	–	354.4	0.220	2.780	8.900	6.370	4721	450.9	7.350	0.260	3.120	0.880
TB-6-4	1655	11.86	134.7	–	633.5	0.210	2.40	7.850	16.58	5257	519.	0.990	1.930	15.40	4.210
TB-6-5	1869	12.33	133.8	–	570.8	0.230	3.010	8.640	13.43	5419	543.1	1.540	0.810	10.25	1.950
TB-6-6	1808	11.88	128.6	0.780	901.3	0.320	2.650	4.560	15.92	5219	534.5	1.260	1.020	9.440	2.120
TB-6-7	2311	11.93	113.5	–	429.3	0.240	3.000	10.88	9.050	4983	457.9	1.190	0.200	5.110	0.740
TB-6-8	1433	13.63	148.3	6.460	550.2	0.120	3.430	9.010	16.59	5174	585.9	1.270	1.940	13.87	5.320
TB-6-9	1721	12.72	144.7	1.950	609.6	0.160	3.050	7.760	18.60	5126	619.4	5.150	1.160	17.30	4.000
TB-6-10	2047	12.28	126.3	0.570	444.6	0.320	2.970	9.190	10.69	4408	506.5	1.880	0.520	7.410	2.090
TB-6-11	2463	12.09	111.7	0.630	324.0	0.180	2.440	9.720	4.710	5075	419.8	0.760	0.400	1.940	0.510
TB-6-12	6318	14.18	132.5	–	627.4	0.700	5.820	–	14.46	4491	466.7	6.620	1.070	11.81	2.600
TB-6-13	1663	11.87	140.5	–	668.9	0.180	3.250	8.510	15.92	5354	571.9	2.650	0.880	10.93	2.380
TB-6-14	1819	11.42	113.1	–	503.1	0.210	2.640	10.53	16.08	4725	428.6	1.560	1.190	15.21	3.490
TB-6-15	1731	11.06	112.9	0.640	383.3	0.220	2.880	6.110	20.29	4372	394.1	1.980	1.730	22.09	5.280
TB-6-16	1951	11.61	115.0	–	329.8	0.230	2.810	12.79	6.470	4683	413.9	0.900	0.450	4.390	1.240
TB-6-17	1654	11.20	115.6	0.640	419.1	0.180	2.790	9.670	12.77	4497	419.1	1.080	1.220	9.980	2.710
TB-6-18	1747	11.29	112.7	0.670	402.8	0.220	2.230	9.440	14.11	4644	422.3	1.100	1.430	11.67	3.650
TB-6-19	1854	12.54	139.1	0.640	515.9	0.230	2.850	9.370	8.940	5808	575.0	0.820	0.400	4.050	1.430
TB-6-20	1720	18.81	158.9	26.09	560.9	0.210	4.410	12.59	17.63	5579	643.5	4.800	1.950	17.19	4.820
TB-6-21	1702	11.42	118.2	–	357.3	0.130	1.950	8.180	18.97	4784	430.0	1.370	0.640	17.07	6.680
TB-6-22	2107	11.41	106.0	0.660	327.1	0.340	2.700	7.270	8.290	4772	433.4	0.790	0.520	5.670	1.470
TB-6-23	2062	11.33	105.6	0.600	409.3	0.220	2.340	9.550	12.47	4719	435.8	0.940	1.030	10.90	3.120
TB-6-24	2084	12.11	112.9	–	478.8	0.260	3.330	8.490	10.92	5297	466.1	1.230	0.860	8.620	1.940
TB-6-25	1780	12.02	134.1	0.700	649.0	0.220	2.390	10.34	18.81	5417	547.3	0.960	2.970	11.63	5.160
Mean	2085	12.32	126.8	3.050	499.5	0.240	2.970	9.060	13.26	4975	496.8	3.260	1.060	10.52	2.890
Max	6318	18.81	158.9	26.09	901.3	0.700	5.820	12.79	20.29	5808	643.5	29.31	2.970	22.09	6.680
Min	1433	11.06	105.6	0.570	324.0	0.120	1.950	4.560	4.710	4372	394.1	0.760	0.200	1.940	0.510

**Table 2 In situ LA-ICP-MS trace element contents in the pyrrhotite in Dongfengnanshan deposit (ppm)**

	Co59	Ni60	Cu65	Zn66	Ga71	Ge72	Se77	Ag107	Cd111	In115	Sn118	Sb121	Pb208	Bi209
TB-6-1	169.0	87.45	1.540	2.820	0.070	12.25	6.680	2.220	–	0.020	0.550	–	6.040	1.960
TB-6-2	184.6	96.61	3.410	1.540	–	13.08	8.240	3.110	–	0.040	–	0.440	10.22	3.900
TB-6-3	147.1	98.08	1.640	–	0.120	12.26	7.960	1.820	–	0.010	0.450	0.100	1.520	0.340
TB-6-4	160.8	103.5	–	0.850	0.280	11.81	17.05	1.750	0.490	–	–	0.150	10.81	3.80
TB-6-5	179.8	89.74	1.890	2.740	0.506	12.64	–	3.570	2.620	0.040	–	0.120	10.89	4.060
TB-6-6	157.0	136.5	2.050	2.050	–	12.08	11.00	2.050	0.760	–	–	0.180	5.710	1.750
TB-6-7	156.1	69.73	1.230	5.600	0.100	12.83	6.110	1.710	–	0.180	2.210	0.050	2.840	0.900
TB-6-8	162.3	251.1	1.490	–	0.080	13.08	6.420	4.900	–	0.050	–	0.100	5.220	2.630
TB-6-9	147.8	89.46	3.210	2.860	0.005	12.78	7.850	1.290	0.430	–	–	–	1.760	0.240
TB-6-10	192.3	102.9	–	1.990	–	13.93	11.10	2.980	–	–	–	–	30.21	3.930
TB-6-11	128.8	122.9	2.550	0.940	0.050	11.12	7.800	2.090	–	0.010	0.330	0.120	3.430	0.450
TB-6-12	154.7	89.75	12.03	68.40	0.390	17.30	6.140	4.650	–	0.870	11.75	0.470	6.510	2.770
TB-6-13	171.5	270.9	1.770	4.490	–	10.83	14.34	3.570	–	0.100	1.050	0.580	7.330	4.530
TB-6-14	163.4	76.69	11.82	4.180	–	13.38	–	1.420	0.480	0.070	–	0.150	2.980	1.040
TB-6-15	171.8	73.67	5.330	2.080	0.090	13.73	10.77	2.060	1.490	0.070	0.730	0.230	3.080	1.480
TB-6-16	150.7	120.7	2.780	10.40	–	12.95	5.790	3.030	–	0.050	2.220	0.090	8.630	3.210
TB-6-17	148.0	47.58	–	2.950	0.380	12.06	15.22	0.840	1	0.050	–	0.230	3.190	1.670
TB-6-18	162.3	118.2	1.380	2.690	0.120	12.79	–	1.590	0.980	–	1.320	–	2.300	0.980
TB-6-19	161.6	136.8	5.530	–	0.120	12.35	15.16	0.610	–	–	–	0.220	0.730	0.310
TB-6-20	164.0	110.8	5.390	3.330	0.140	13.62	10.08	1.770	10.20	0.030	–	0.150	9.140	2.540
TB-6-21	155.5	124.6	0.980	1.470	0.090	11.51	9.920	1.050	0.820	0.050	0.720	–	2.470	1.120
TB-6-22	156.8	128.6	0.860	2.740	0.330	12.57	11.01	1.600	1.420	0.030	–	0.310	2.210	1.070
TB-6-23	162.3	95.75	5.430	–	0.200	12.46	6.120	0.890	0.490	0.040	–	0.330	1.930	0.370
TB-6-24	157.6	124.5	1.780	1.970	0.170	13.25	–	1.900	0.280	0.030	–	0.170	6.910	2.990
TB-6-25	170.8	116.4	13.24	4.020	0.220	12.02	–	10.80	–	–	–	0.590	7.920	2.340
Mean	161.4	115.3	3.970	6.200	0.190	12.75	9.740	2.530	1.650	0.097	2.130	0.240	6.160	2.020
Max	192.3	270.9	13.24	68.40	0.560	17.30	17.05	10.80	10.20	0.870	11.75	0.590	30.21	4.530
Min	128.8	47.58	0.860	0.850	0.050	10.83	5.790	0.610	0.280	0.010	0.330	0.050	0.730	0.240

**Table 3 In situ LA-ICP-MS trace element contents in the chalcopyrite in Dongfengnanshan deposit (ppm)**

	Co59	Ni60	Cu65 (wt%)	Zn66	Ga71	Ge72	Se77	Ag107	Cd111	In115	Sn118	Sb121	Tl205	Pb208	Bi209
TB-6-1	2.580	0.890	33.49	540.6	0.200	5.840	11.17	551.0	8.930	58.59	140.0	0.430	0.080	2.370	0.640
TB-6-2	2.130	2.570	35.58	570.1	0.180	6.710	21.25	853.5	14.79	64.57	149.0	1.120	3.080	5.310	1.700
TB-6-3	3.020	–	33.26	492.7	0.120	6.300	19.85	679.1	9.730	59.50	84.39	0.850	0.760	13.07	2.880
TB-6-4	3.480	1.730	32.97	604.5	0.090	5.630	14.60	612.8	8.890	66.38	187.1	0.580	–	3.130	0.910
TB-6-5	2.960	1.120	33.24	719.8	0.130	6.200	12.80	634.6	9.570	61.09	287.6	0.380	0.060	2.290	0.590
TB-6-6	4.100	1.100	32.82	645.0	0.150	5.940	15.98	583.4	9.690	58.98	232.7	0.590	0.050	3.990	1.290
TB-6-7	2.980	–	34.43	720.5	–	5.310	23.00	691.1	11.19	62.93	219.3	1.290	0.120	7.490	2.780
TB-6-8	7.730	–	32.57	477.4	0.090	6.530	24.65	613.5	7.410	74.54	63.12	1.390	0.040	7.970	1.860
TB-6-9	7.730	–	32.41	672.6	0.120	6.400	17.34	634.0	9.440	83.31	233.2	1.150	–	4.310	0.960
TB-6-10	8.540	2.190	33.38	561.3	0.210	5.540	20.15	613.6	6.320	61.24	238.1	0.890	0.060	3.480	0.840
TB-6-11	7.220	2	31.20	552.1	0.090	6.410	13.71	589.9	6.590	67.12	71.29	2.040	0.330	15.63	4.250
TB-6-12	7.410	–	33.42	648.3	0.110	6.680	17.52	629.4	7.440	62.15	170.1	0.970	–	4.600	2.270
TB-6-13	2.350	2.560	34.74	454.2	0.140	6.730	12.24	783.5	13.99	70.15	67.37	1.320	2.050	25.37	7.100
TB-6-14	2.450	0.970	29.80	293.2	0.110	6.600	9.920	543.9	7.490	73.59	69.38	0.970	3.430	16.03	3.760
TB-6-15	2.380	2.200	31.52	394.7	0.180	5.540	10.45	624.5	7.480	74.99	51.58	0.390	0.030	4.240	1.030
TB-6-16	2.210	3.000	33.41	557.5	0.200	8.570	10.83	852.1	12.33	63.53	107.2	1.660	1.850	17.16	4.960
TB-6-17	1.150	–	33.09	528.7	0.300	5.610	19.93	696.2	9.970	75.50	86.87	0.860	0.250	6.860	1.880
TB-6-18	0.910	2.410	31.17	404.4	0.130	5.770	14.64	603.5	6.850	71.66	42.35	1.480	2.980	22.12	7.140
TB-6-19	3.190	–	33.05	393.6	0.110	6.490	13.44	636.3	8.050	62.46	71.81	0.450	0.180	4.480	0.770
TB-6-20	2.760	1.580	29.65	353.9	0.530	7.410	12.67	591.3	9.550	60.80	132.3	0.960	2.020	6.130	1.400
TB-6-21	2.140	–	35.65	497.0	–	4.490	21.27	789.6	10.88	78.75	76.84	0.880	0.140	7.310	1.670
TB-6-22	2.570	–	32.87	441.7	0.210	5.750	13.06	619.0	9.800	72.83	53.37	1.020	0.430	17.88	2.460
TB-6-23	5.090	1.560	33.15	322.3	0.100	6.320	13.20	600.0	6.290	69.28	45.89	0.390	0.160	2.580	0.640
TB-6-24	3.910	–	33.29	473.4	0.140	5.210	13.45	637.0	6.930	66.62	167.5	0.220	–	1.130	0.310
TB-6-25	4.630	–	34.86	534.7	0.160	6.530	–	805.0	13.26	64.56	105.1	0.790	–	6.050	1.550
Mean	3.820	1.850	33.00	514.2	0.170	6.180	15.71	658.7	9.310	67.40	126.1	0.920	0.910	8.440	2.230
Max	8.540	3.000	35.65	720.5	0.530	8.570	24.65	853.5	14.79	83.31	287.6	2.040	3.430	25.37	7.140
Min	0.910	0.890	29.65	293.2	0.090	4.490	9.920	543.9	6.290	58.59	42.35	0.220	0.030	1.130	0.310

Note: – : &lt;minimum detection limit.



**Table 4 Mean concentration (mainly ppm) in sulfides from different genetic types of deposits**

Genetic type	Name (spot number)	Minerals	Mn	Fe	Co	Ni	Cu	Concentration							References	
								Zn	Ga	Ge	Cd	In	Sn	Se		Pb
VMS	Laochang (30)	Sphalerite	3060	13.10wt%	0.9	0.19	267	–	23	4.15	8739	200	7.01	1.85	26	Ye et al., 2012
	Vorta, Romania (8)	Chalcopyrite	0.27	–	1.5	<mdl	–	258	1.0	–	1.2	0.1	0.3	<mdl	8	George et al., 2017
SEDEX	Dabaoshan (26)	Sphalerite	2174	11.65wt%	2.13	<mdl	787a	–	29.22	3.28	5609	227	11.99a	–	27.3a	Ye et al., 2011
	Dabaoshan (7)	Pyrrhotite	11.3	–	15.0	6.84	431	8.78	0.5	3.05	–	0.01	0.74	19.4	16.2	Liu et al., 2019
	Kapp Mineral, Norway (9)	Chalcopyrite	14	–	0.16	0.26	–	10.65	0.16	–	3.3	1.4	15	2.5	<mdl	George et al., 2018
Skarn	Hetaoping	Sphalerite	2073	5.28wt%	212	<mdl	622a	–	0.53	2.83	4737	0.048	<mdl	31.4a	37.4a	Ye et al., 2011
	Ocna de Fier (35)	Sphalerite	4473	2.62wt%	604	0.88	842	–	0.75	1.01#	5852	21.89	5.58	0.37	3467*	Cook et al., 2009
	Hongshan(20)	Pyrrhotite	0.51	–	0.18	4.94	0.65	0.39	–	–	0.03	–	0.16	15.4	2.32	Leng, 2017
	Luotuooshan (32)	Pyrrhotite	157.62	6.01wt%	57.75	19.24	3.32	206.19	0.491	3.34	1.80	0.357	0.46	4.41	0.94	Xing et al., 2017
	Baita Bihor	Chalcopyrite	4.5	–	10.5	0.695	–	829.5	0.44	–	26.5	145.5	149	72	3.15	George et al., 2018
Epithermal	Torogia Tga–1 (6)	Sphalerite	763	7.16wt%	1	<mdl	1644*	–	4	1#	7751	93	<mdl	4	<mdl	Cook et al., 2009
	Kochbulak (10)	Chalcopyrite	0.88	–	0.04	0.02	–	915	0.17	–	19	2.7	11	31	1.5	George et al., 2018
MVT–type	Niujiatong (18)	Sphalerite	28.64a	1.19wt%	<mdl	<mdl	42.58	–	11.1	82.18	10302	0.1	1.58a	0.51	335a	Ye et al., 2011
	Mengxing(18)	Sphalerite	147a	0.53 wt%	2.37	<mdl	88.6a	–	2.20	16.13a	12135	–	0.18	0.03	712	Ye et al., 2011

	Jinding (24)	Sphalerite	184a	0.13wt%a	5.43a	0.02	62.9a	–	2.52a	11.35	17940	<mdl	<mdl	<mdl	1425	Ye et al., 2011
	Tres Maria (22)	Sphalerite	27.87	6.18wt%	0.31	0.57	19.23	–	12.33	704.2	5109.5 <sup>#</sup>	0.15	1.88	3.08	2140	Cook et al., 2009
Porphyry	Bor (10)	Chalcopyrite	2.4	–	0.05	–	–	65	0.14	–	0.77	0.69	16	2.4	12	George et al., 2018
Cu–Ni sulfide deposit	Jinchuan (3)	Chalcopyrite	–	–	108.3	0.3wt%	30.57wt%	534	–	–	6.15	–	–	225.1	–	Chen et al., 2015
	Creighton (80)	Pyrrhotite	–	–	152	0.9wt%	0	1.75	–	–	0.13	–	0.44	105.69	1.49	Dare et al., 2010

Note: –: not analyzed; \*: Standard deviation>mean concentration value; Ge<sup>#</sup>: Absolute concentrations (in ppm terms) must be considered as approximate only due to uncertainties in Ge content of standard.  
a: the mean includes at least one spot in which the element in question appears as inclusions on the LA–ICPMS profile.

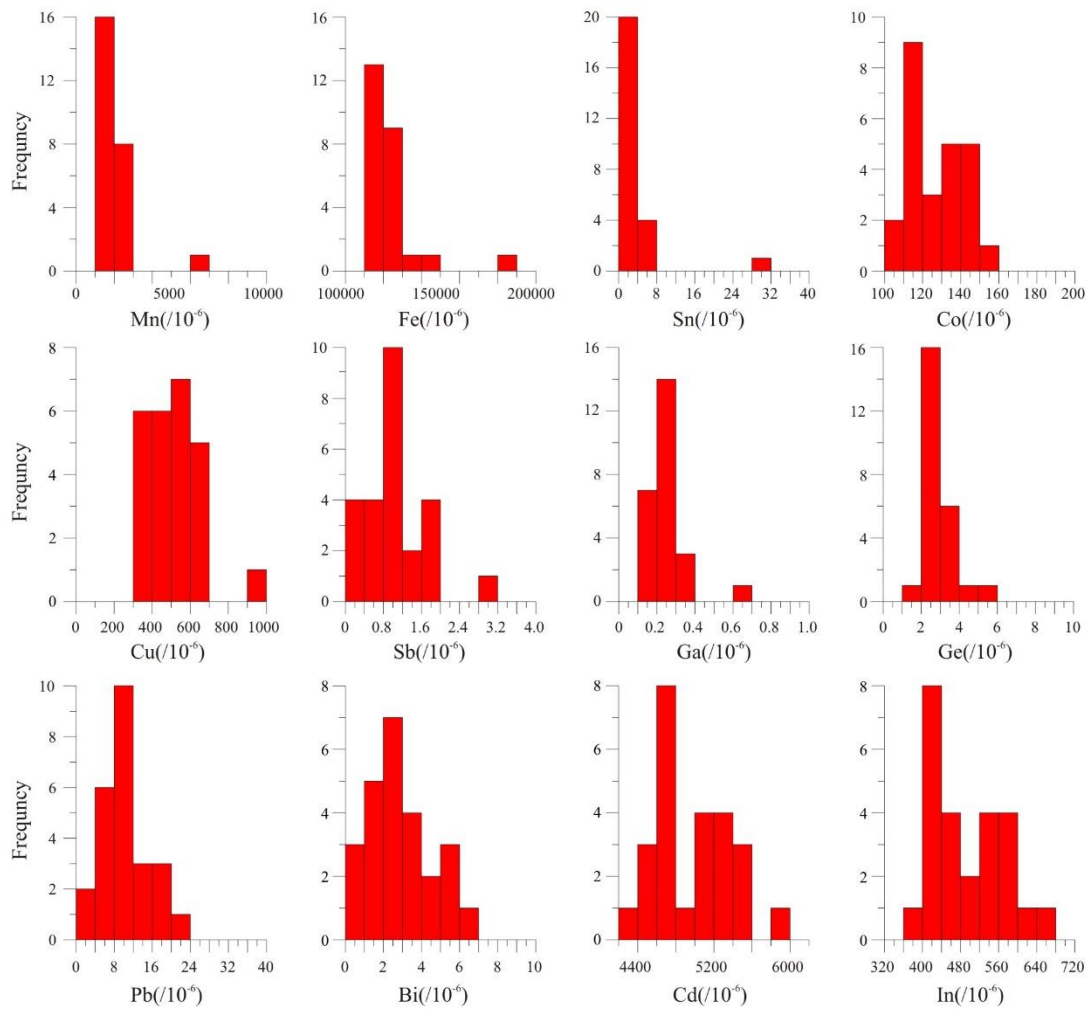


Fig. 4. Distribution histograms of elements in sphalerite as determined by LA-ICP-MS.

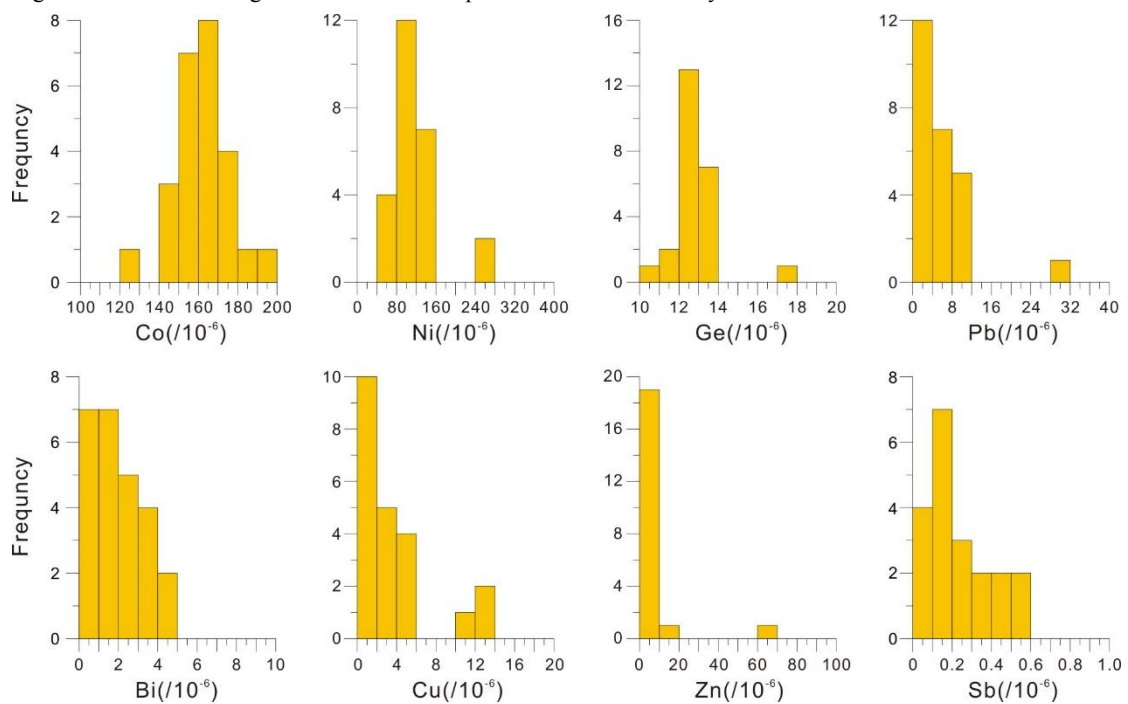


Fig. 5. Distribution histograms of elements in pyrrhotite as determined by LA-ICP-MS.

VMS-type deposits (e.g., Sulitjelma, with a mean of 431 ppm, George et al., 2018). Cd concentration is similar to which in recrystallized VMS-type deposit (e.g., Sulitjelma, with a mean of 17.16 ppm, George et al., 2018). The concentration of Cu varies from 296,523 ppm to 356,499 ppm, with an average of 330,007 ppm, which is relatively stable. The range in Ge, Ag, and In concentrations are slightly wider (Fig.6);  $\omega(\text{Ge})$ ,  $\omega(\text{Ag})$ , and  $\omega(\text{In})$  are 4.49–8.57 ppm, 543–853 ppm, and 58–83 ppm, respectively. The concentrations of Pb, Bi, and Sb vary at 1.13–25.37 ppm, 0.31–7.14 ppm, and 0.22–2.04 ppm, respectively.

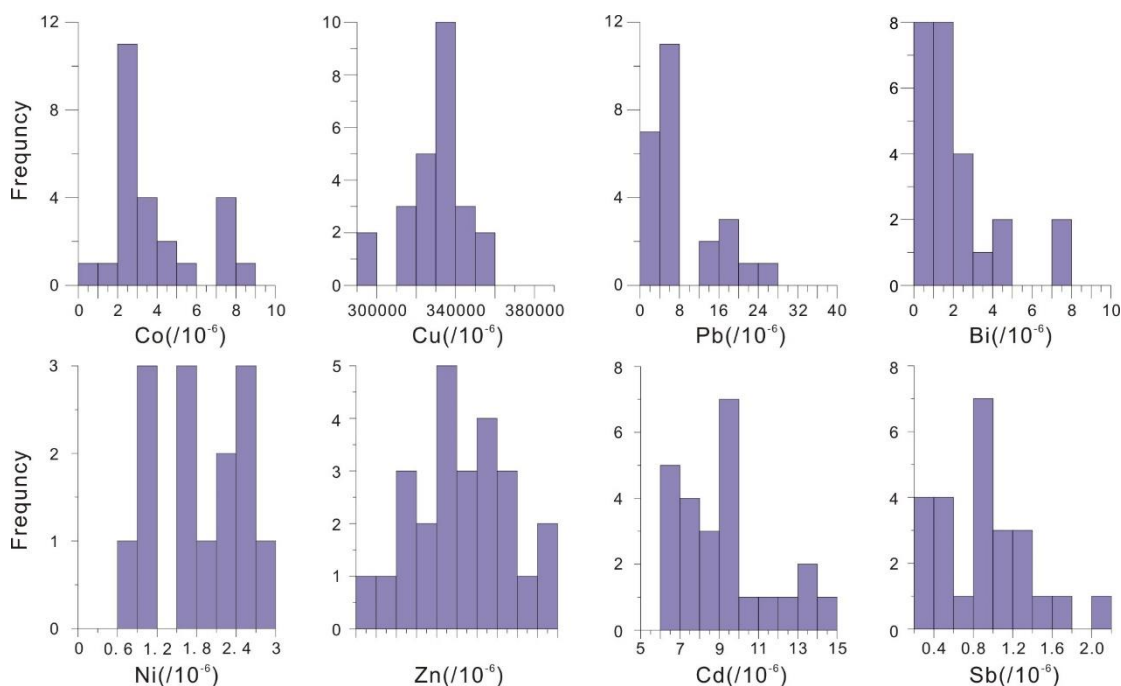


Fig. 6. Distribution histograms of elements in chalcopyrite as determined by LA-ICP-MS.

#### 4.2 S–Pb Isotopes

The S isotope compositions of four pyrrhotite samples in the Dongfengnanshan stratiform ore bodies are shown in Table.5. The  $\delta^{34}\text{S}_{\text{V-CDT}}$  value of pyrrhotite ranges from 1.0‰ to 2.0‰, with an average of 1.55‰. These values are similar to those of sulfides measured in previous research (Li et al., 1991).

**Table 5 Sulfur isotope compositions of sulfides from Dongfengnanshan deposit**

Deposit/strata	Sample No.	minerals	$\delta^{34}\text{S}/\text{‰}$			References
			Value	Range	Mean	
Dongfengnanshan	7TB-6Po1	Pyrrhotite	1.90	1.0~2.0	1.55	This study
	7TB-6Po2	Pyrrhotite	1.30			
	7TB-6Po3	Pyrrhotite	1.00			
	7TB-6Po4	Pyrrhotite	2.00			
Dongfengbeishan		Molybdenum		0.2~2.8	1.76	Zhang et al.,2013
		Molybdenum		-1.1~2.8	1.46	Gao et al., 2010
		Pyrrhotite		1.2~1.6	1.40	Wang et al.,2017
		Pyrrhotite		-0.9~-0.8	-0.85	Wang et al.,2017
Lishan		Chalcopyrite		-2.4~-2.1	-2.28	Wang et al.,2017
		Galena		-4.0~-1.5	-2.71	Sun et al.,2006
		Sphalerite		-2.0~-1.0	-1.61	Sun et al.,2006
		Pyrrhotite		-1.3~-1.0	-1.15	Wang et al.,2017
Xinxing		Chalcopyrite		-2.3~-1.3	-1.80	Wang et al.,2017
		Galena		-2.7~-2.6	-2.65	Wang et al.,2017
		Sphalerite		-2.0~-1.4	-1.70	Sun et al.,2006
Miaoling Formation		Volcanic rock		-1.2~-1.7		Sun et al.,2006

The S isotope composition of sulfides can reflect the source of the ore-forming materials in metal deposits; however, the  $\delta^{34}\text{S}$  value does not fully represent the total  $\delta^{34}\text{S}$  value of the ore-forming hydrothermal fluid. The total value is also affected by physical and chemical conditions such as oxygen fugacity, pH, and fluid temperature (Ohmoto, 1972; 1986). The sphalerite is enriched in Fe, at 11.2%–18.8% (Table.1), which suggests that the stratiform ore bodies formed under low oxygen fugacity conditions; According to previous research,  $\delta^{34}\text{S}_{\text{py}} > \delta^{34}\text{S}_{\text{sp}} > \delta^{34}\text{S}_{\text{Gn}}$  in the ore deposit indicates that the S isotope essentially reaches the fractionation equilibrium during the ore-forming process; thus the  $\delta^{34}\text{S}$  value of sulfides is approximately equal to the  $\delta^{34}\text{S}$  value of the ore-forming hydrothermal fluid (Ohmoto et al., 1997)

The analysis results of the Pb isotope of four pyrrhotite samples in the stratiform ore bodies, are shown in Table.6. The  $^{206}\text{Pb}/^{204}\text{Pb}$  is 18.635–18.671, with an average of 18.654; the  $^{207}\text{Pb}/^{204}\text{Pb}$  is 15.583–15.608, with an average of 15.593; the  $^{208}\text{Pb}/^{204}\text{Pb}$  is 38.291–38.352, with an average of 38.317. The results were input into GeoKit software to calculate other parameters of the Pb isotope. The ranges of  $\mu$  and  $\omega$  vary at 9.41–9.45 and 34.52–34.89, respectively.

**Table 6 Lead isotope compositions of sulfides from Dongfengnanshan deposit**

Deposit	Sample NO.	Minerals/Rocks	$^{206}\text{Pb}/^{204}\text{Pb}$	$^{207}\text{Pb}/^{204}\text{Pb}$	$^{208}\text{Pb}/^{204}\text{Pb}$	References
Dongfengnanshan	7TB-6Po1	Pyrrhotite	18.658	15.598	38.332	This study
	7TB-6Po2	Pyrrhotite	18.653	15.583	38.293	
	7TB-6Po3	Pyrrhotite	18.635	15.583	38.291	
	7TB-6Po4	Pyrrhotite	18.671	15.608	38.352	
Dongfengbeishan		Galena	18.384–18.695	15.682–15.729		Sun et al., 2006
		Galena	18.6–18.685	15.711–15.723	39.101–39.189	Zhang et al., 2013
Lishan		Galena	18.073–18.363	15.397–15.532		Sun et al., 2006
		Galena	18.318–18.322	15.568–15.571	38.178–38.186	Zhang et al., 2013
Xinxing		Galena	18.208–18.463	15.372–15.437		Sun et al., 2006
		Galena	18.174–18.313	15.379–15.442	37.554–38.821	Zhang et al., 2013
		Galena	18.317–18.323	15.563–15.569	38.165–38.183	Zhang et al., 2013
		Galena	18.356	15.443		Zhang et al., 2013
		Granodiorite	18.277–18.396	15.547–15.578	38.44–38.5	Sun et al., 2006
		Marble	18.063–18.140	15.370–15.414	37.289–37.866	Sun et al., 2006

## 5 Discussions

### 5.1 Formation Temperature of Sulfides in Stratiform Ore Bodies

The trace element distributions in sphalerite can reflect the formation temperature. Generally, the high-temperature sphalerite is significantly enriched in Fe, Mn, In, Co, and other elements, with high  $\text{In}/\text{Ga}$ ,  $\text{Zn}/\text{Cd} > 600$ , and  $\omega(\text{Fe})$  usually  $> 10\%$ , belonging to Fe-sphalerite. Whereas, the low-temperature sphalerite is enriched in Cd, Ga, and Ge, with low ratio value of  $\text{In}/\text{Ge}$  and  $\text{Zn}/\text{Cd} < 100$ .

The sphalerite in the stratiform ore bodies of the Dongfengnanshan deposit is characterized by high contents of Fe, In, Mn, and Co, and limited contents of Ga and Ge, which are similar to the VMS-type deposits associated with intermediate formation temperatures such as the Laochang Pb–Zn deposit, with Fe at 13.1wt%, Mn at 3060 ppm, and In at 200 ppm (Ye et al., 2012), contrast to those of low-temperature hydrothermal deposits such as the Huize Pb–Zn deposit, with Cd at 1360 ppm, Ga at 4.08 ppm, and Ge at 31.58 ppm (Zhang et al., 2016).

The Cd/Zn ratio in the chalcopyrite is controlled generally by the crystallization temperature. Generally, at relatively higher temperatures, chalcopyrite tends to be enriched in Cd relative to Zn (George et al., 2018). The Cd/Zn binary diagram, shown in Fig.7, indicates that the chalcopyrite in the ore bodies of the Dongfengnanshan deposit has a relatively moderate Cd/Zn ratio. In addition, the majority of samples falls within the range of the recrystallized VMS-type deposit and partially in the range of the skarn deposit, implying an intermediate formation temperature.

### 5.2 Ore Sources

The previous research data in the Tianbaoshan ore district indicate the  $\delta^{34}\text{S}$  values of the sulfide from the skarn Pb–Zn–Cu mineralization (SM) at Lishan deposit and the cryptoexplosive breccia-type Pb–Zn–Cu mineralization (CBM) at Xinxing are similar ( $-4.0\%$  to  $-0.8\%$  with mean of  $-2.16\%$  and

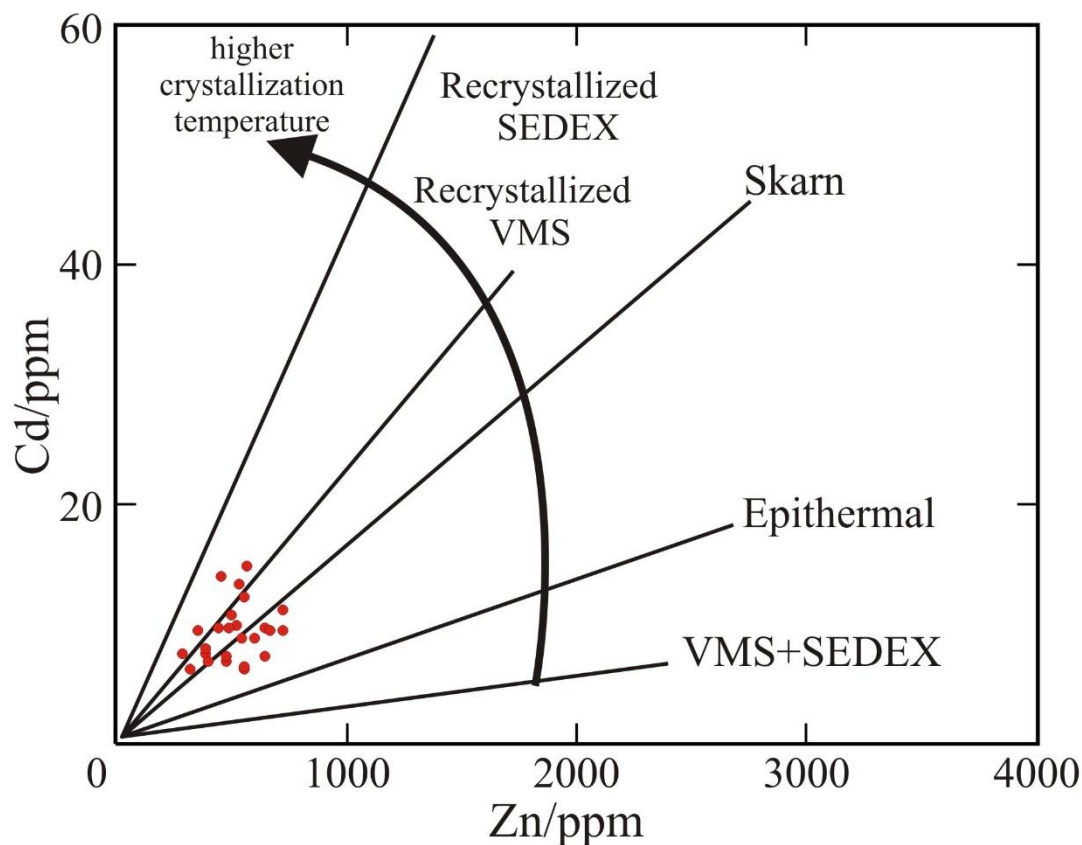


Fig. 7. Binary diagram of Cd versus Zn for hydrothermal chalcopyrite (modified from Charley et al., 2019).

−2.7‰ to −1‰ with mean of −2.31‰, respectively) (Wang et al., 2017a). The sulfur sources in the two types of mineralization may be derived from the mixing of magma during Middle Permian. The  $\delta^{34}\text{S}$  values (0.2‰–2.8‰) of the sulfide in the quartz–vein type Mo mineralization (QVM) in the Dongfengbeishan are higher than those in the SM, CBM and volcanic rocks of the Miaoling Formation, and the early Yanshanian granitoid is inferred as the sulfur source.

The  $\delta^{34}\text{S}$  value of sulfides in the stratiform ore bodies in the Dongfengnanshan lies in a narrow range of 1.0‰ to 2.0‰, higher than those of SM and CBM, and lower than those of QVM (Fig.8). Therefore, we can exclude the Hercynian granodiorite and the Yanshanian granitoid as the sulfur source. Moreover, the  $\delta^{34}\text{S}$  value of the altered volcanic rocks in the ore district has been reported as and −1.2‰ to 1.7‰ (Sun et al., 2006), which are close to those of the sulfides in the stratiform ore bodies. The data suggest that the sulfur might have originated from volcanic rocks of the Early Permian Miaoling Formation. All these reflect that the sulfur in the Dongfengnanshan stratiform ore bodies is related to the degassing of circular–leaching seawater during the formation of the ore–bearing strata (Ohmoto et al., 1983).

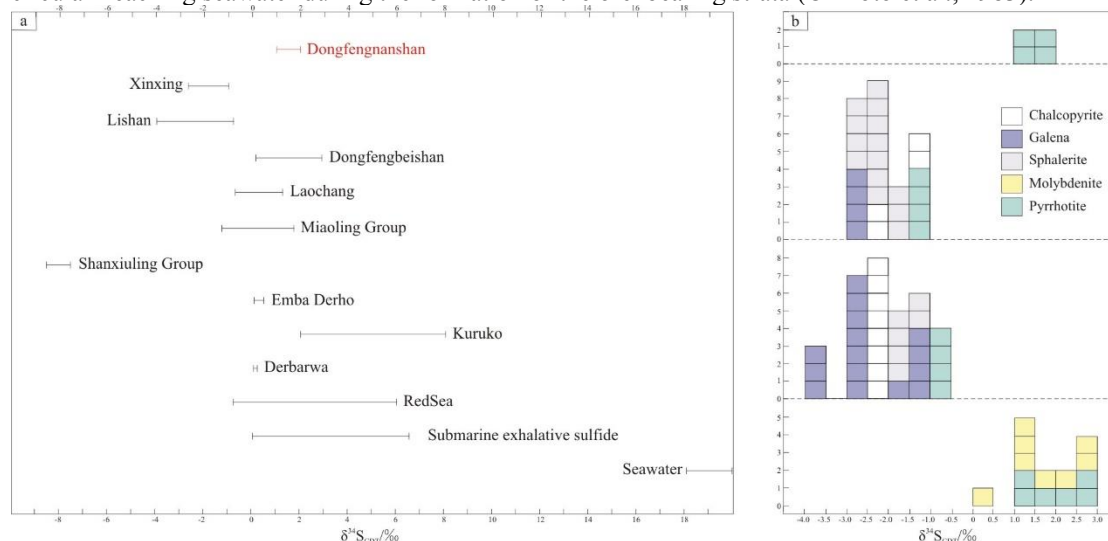


Fig. 8. (a) Sulfur isotopic compositions of sulfide from Tianbaoshan ore district and some typical VMS deposits. (b) Histograms of sulfur isotope data in the Tianbaoshan ore district (modified from Wang et al., 2017a).

The Pb isotope of sulfides is an important factor for tracing the source of ore-forming materials (Wu et al, 2002). Stacey et al. (1983) summarized that, in the tectonic discriminant diagram (Fig.9), if sample point is above the evolution line of the orogenic belt, lead is contained in the upper crust component; that near the evolution line indicates that the lead has a mixed source; and that below the evolution line indicates that the lead was derived from the mantle or the lower crust. The lead isotope compositions in the SM and CBM were derived from mixture of the Shanxiuling Formation and the post-magmatic hydrothermal fluids related to the cooling and fractional crystallization of the granodiorite magma and the lead in the QVM has the same source as the sulfur, the Yanshanian magmatic activity (Wang et al., 2017a).

In the Fig.9, samples from the stratiform ore bodies in the Dongfengnanshan are distributed in the vicinity of the growth line of the orogenic belt, with the characteristics of Pb from the orogenic belt, indicating that the Pb has a mixed source (Stacey et al., 1983). A lower  $\mu$  ( $<9.58$ ) reflects lead from the upper mantle or lower crust, and a higher  $\mu$  value reflects that from the upper crust (Kamona et al., 1999). The  $\mu$  value of the sulfides in this study ranges from 9.41 to 9.47, reflecting a mixed lead source. These results differ significantly from the lead isotope characteristics of marble and are close to those of the widely distributed granodiorite (Sun et al., 2006). In summary, it can be inferred that the Pb of the sulfides in the stratiform ore bodies has a mixed source of mantle and crust, with contribution from both the Hercynian granodiorites and the volcanic rocks of the Miaoling Formation.

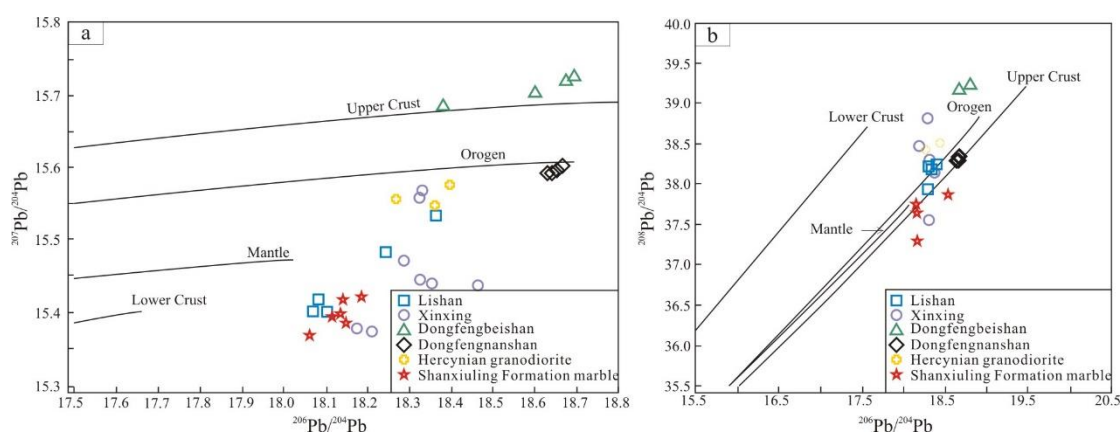


Fig. 9. Lead isotopic compositions of sulfides and wall-rocks in the Tianbaoshan ore district (modified from Wang et al., 2017a).

(a)  $^{207}\text{Pb}/^{204}\text{Pb}$  vs.  $^{206}\text{Pb}/^{204}\text{Pb}$ ; (b)  $^{208}\text{Pb}/^{204}\text{Pb}$  vs.  $^{206}\text{Pb}/^{204}\text{Pb}$ .

### 5.3 Ore Genesis of Stratiform Ore bodies

As mentioned above, the stratiform ore bodies are hosted in the interlayer of intermediate-acidic volcanic rocks and limestone of the Early Permian Miaoling Formation, and concordant with the wall rocks. The Cu polymetallic mineralization occurs in the volcanic sedimentary-exhalative rocks with no or weak wall-rock alterations. The major ore structures are banded and massive. These properties are corresponding to those of VMS-type deposits. With respect to the vein-type ore bodies, they are hosted near the contact zone of the diorite intrusion and the strata, with skarn diagnostic minerals such as garnet. Therefore, it is considered to be skarn-type preliminarily.

According to the geological settings, generally, VMS-type deposits can be divided into two categories: one formed in the mid-oceanic ridge with slow or rapid expansion and is set in the oceanic crust, and its ore-bearing rocks are mainly oceanic tholeiitic, characterized by Cu or Cu-Zn mineralization. The other is distributed in the island arc or active continental margin including island arc rift, continental rift, and back-arc basin, and the ore-hosting rocks are mainly bimodal volcanic rocks, characterized by Cu-Pb-Zn mineralization. In the Dongfengnanshan deposit, weighted mean U-Pb age of the zircon from the ore-bearing volcanic rock is  $296 \pm 2.6$  MaBP (unpublished data), and Zhang et al. (2004) supposed that the Permian tonalite at 285 MaBP was probably emplaced during the subduction of the Paleo-Asian Ocean beneath the NCC. Therefore, the stratiform ore bodies are likely to be formed in the back-arc basin in the background of subduction.

Trace elements concentrations of different sulfides demonstrate that the Fe, In, and Mn concentrations of sphalerite in low-temperature hydrothermal deposits are low and that Ga, Ge and Cd have high concentrations (Table.4). In the skarn deposits, Co and Mn have a high concentration in contrast to the low concentrations of Fe and In, and Co is usually one to two orders of magnitude

higher than that in other types of deposits. The sphalerite in the VMS-type deposits has high Fe, In, Mn, and Sn concentrations and low Ga and Ge concentrations (Tu et al., 2004; Cook et al., 2009; Ye et al., 2011). The sphalerite in the stratiform ore bodies of the Dongfengnanshan deposit is characterized by high Fe, Mn and In concentrations and low concentrations of Ga and Ge, which is similar to that in the sphalerite of the VMS-type deposits, and distinctly different from those in the skarn, epithermal and MVT deposits.

Chen (1995) summarized a Co–Ni relationship diagram of the pyrrhotite and chalcopyrite in Cu deposits. In addition, Zhang (1987) identified the genetic types of Pb–Zn deposits by using trace elements of sphalerite and galena. Moreover, many scholars both in China and abroad have drawn diagrams of trace elements (Cook et al., 2009, 2016; Ye et al., 2011, 2012; Hu et al., 2014; Leng, 2017; George et al., 2018; Charley et al., 2019). In different binary diagrams of trace elements (Fig.10), the sulfides from the stratiform ore bodies are similar to Laochang (VMS-type deposit) and Dabaoshan (SEDEX-type deposit) in South China, and differ significantly from MVT and skarn deposits. An interesting fact is that the Co concentration of sulfides in the stratiform ore bodies is higher than that of the VMS-type deposits, but similar to that in skarn deposits. This result may be explained by the transformation of the stratiform ore bodies by the late Hercynian ore-bearing hydrothermal fluid in the ore district, which caused an abnormal enrichment in Co.

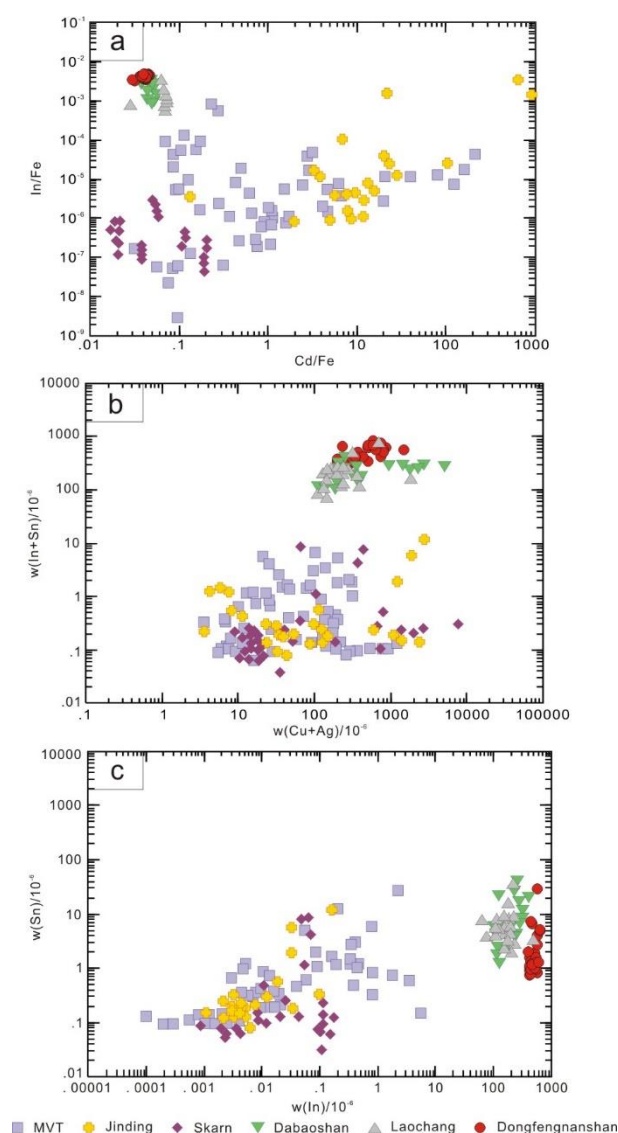


Fig. 10. Binary plots of Cd/Fe vs. In/Fe, (Cu+Ag) vs. (In+Sn), In vs. Sn in sphalerite from Dongfengnanshan and other Pb-Zn deposits in China (modified from Ye et al., 2011).



George et al. (2018) supposed that hydrothermal chalcopyrite with a higher Cd/Zn ratio occurs in recrystallized VMS-type deposits. In addition, Charley et al. (2019) summarized the trends of Cd and Zn in different genetic types by using a binary diagram of Cd versus Zn for hydrothermal chalcopyrite (Fig.7). The chalcopyrite samples from the Dongfengnanshan deposit are located mainly near the recrystallized VMS-type and skarn deposits. The conclusion is consistent with that from sphalerites.

Previous research has shown that the  $\delta^{34}\text{S}$  value of VMS-type deposits is characterised by a concentration at 0‰ (Houston, 2009), for example, the Kuruko deposit, at 2‰ to 8‰ (Ohmoto, 1996); the Red Sea deposit, at -0.8‰ to 6‰ (Mao et al., 2015); the Laochang deposit, at -0.69‰ to 1.32‰ (Zhang et al., 2017); the Emba Derho deposit, at 0.08‰ to 0.48‰ (Cheng et al., 2017); and the Debarwa deposit, at 0.01‰ to 0.25‰ (Cheng et al., 2017). The  $\delta^{34}\text{S}$  value of the pyrrhotite in the Dongfengnanshan deposit is between 1‰ and 2‰, which is similar to that in VMS-type deposits worldwide. The lead in the VMS-type deposits originate from deep regions, mainly from the upper mantle or the lower crust (Liu et al., 1999), and that in the Dongfengnanshan deposit originates from deep regions as well as granodiorites and volcanic rocks. Analogous to modern submarine hydrothermal ore bodies, it is believed that the magmatic fluids carrying ore-forming elements and volatiles escaped from deep-source magma and were released during the early Permian submarine volcanism. Seawater at high temperatures underwent frequent material exchanges with volcanic rocks, and the ore-forming elements were gradually enriched to form stratiform ore bodies.

## 6 Conclusions

(1) The Dongfengnanshan deposit in the Tianbaoshan ore district occur two types of ore bodies, the stratiform and vein-type. The stratiform ore bodies are hosted in the intermediate-acidic volcanic rocks and limestone of the Early Permian Miaoling Formation. The ore structure is mainly banded, the ore texture is granular and weakly metasomatic, and with no or weak wall-rock alterations.

(2) In situ LA-ICP-MS trace element analysis of the sulfides in the stratiform ore bodies showed that the sphalerite belongs to Fe-sphalerite, which is enriched in Fe, Mn, In, and Co and depleted in Cd, Ga, and Ge. The concentrations of Co and Ni in the pyrrhotite are less than those of the Cu-Ni deposits and higher than those of the skarn deposits. The Zn/Cd ratio of the chalcopyrite indicates the intermediate formation temperature.

(3) The sulfur of the sulfides in the stratiform ore bodies was originated from the volcanic rocks of the Early Permian Miaoling Formation. The lead was derived mainly from the orogenic belt and has a mixed source of the Hercynian granodiorites and volcanic rocks of the Miaoling Formation.

(4) A comprehensive comparison of the ore-forming geological conditions, trace element characteristics, and S-Pb isotopic characteristics of different types of deposits, reveals that the genetic type of the stratiform ore bodies in the Dongfengnanshan deposit is VMS-type, and associated with the early Permian submarine volcanism in this area.

## Acknowledgements

This study is supported by the National Natural Science Foundation of China (NSFC) (No. 41772062). The authors thank ZHANG Bo and other colleagues from Jilin Hanfeng Mining Co. Ltd. for their generous support in field works.

## References

- Cai, J.H., Zhou, W.N., and Zhang, J.Z., 1996. Typomorphic characteristics of sphalerites in the Yinshan copper, lead and zinc polymetallic deposit, Jiangxi. *Journal of Guilin Institute of Technology*, 16(4): 370–375 (in Chinese with English abstract).
- Cao, H.H., Xu, W.L., Pei, F.P., Guo, P.Y., and Wang, F., 2012. Permian tectonic evolution of the eastern section of the northern margin of the North China Plate: constraints from zircon U-Pb geochronology and geochemistry of the volcanic rocks. *Acta Petrologica Sinica*, 28: 2733–2750 (in Chinese with English abstract).
- Cao, H.H., Xu, W.L., Pei, F.P., Wang, Z.W., Wang, F., and Wang, Z.J., 2013. Zircon U-Pb geochronology and petrogenesis of the Late Paleozoic–Early Mesozoic intrusive rocks in the eastern segment of the northern margin of the North China Block. *Lithos*, 170–171: 191–207.
- Chai, P., Sun, J.G., Xing, S.W., Men, L.J., and Han, J.L., 2015. Early Cretaceous arc magmatism and high-sulphidation epithermal porphyry Cu–Au mineralization in Yanbian area, Northeast China: the Duhuangling example. *International Geology Reviews*, 57: 1267–1293.
- Chai, P., Sun, J.G., Hou, Z.Q., Xing, S.W., and Wang, Z.Y., 2016a. Geological, fluid inclusion, H–O–S–Pb isotope, and Ar–Ar geochronology constraints on the genesis of the Nancha gold deposit, southern Jilin Province, northeast China. *Ore Geology Reviews*, 72: 1053–1071.
- Chai, P., Sun, J.G., Xing, S.W., Chen, L., and Li, L., 2016b. Ore geology, fluid inclusion, and  $^{40}\text{Ar}/^{39}\text{Ar}$  geochronology constraints on ore genetic type of the Yingchengzi gold deposit, southern Heilongjiang Province, NE China. *Ore Geology Reviews*, 72: 1022–1036.
- Chai, P., Sun, J.G., Xing, S.W., Chen, L., and Han, J.L., 2016c. Geochemistry, zircon U–Pb analysis, and fluid inclusion  $^{40}\text{Ar}/^{39}\text{Ar}$  geochronology of the Yingchengzi gold deposit, southern Heilongjiang Province, NE China. *Geological Journal*, 65: 502–522.
- Charley, J.D., Hugo, D., Philippe, P., Sarah, J.B., Martin, R., Dany, S., Ben, J.C., Jean, P.A., and Eduardo, T.M.,

2019. Applications of trace element chemistry of pyrite and chalcopyrite in glacial sediments to mineral exploration targeting: Example from the Churchill Province, northern Quebec, Canada. *Journal of Geochemical Exploration*, 196: 105–130.
- Chen, C., 2017. Late Paleozoic–Mesozoic tectonic evolution and regional metallogenic regularity of the eastern Yanbian area, NE China (Ph.D. thesis). Changchun: Jilin University, 1–201 (in Chinese with English abstract).
- Chen, C., Ren, Y.S., Wu, T.T., Yang, Q., and Shang, Q.Q., 2019. Genesis and mineralization age of the quartz–vein–type scheelite deposits in Eastern Yanbian, Northeast China: Constraints on the regional tectonic setting. *Geological Journal*, 54(2).
- Chen, D., 2009. Ore bodies and metallogenic model of Tianbaoshan Cu–Pb–Zn–Mo polymetallic deposit, Yanbian (Master thesis). Changchun: Jilin University, 1–76 (in Chinese with English abstract).
- Chen, D.F., 1995. Characteristics of main metallic minerals in some copper–nickel sulfide deposits of China. *Acta Petrologica et Mineralogica*, 14(4): 345–354 (in Chinese with English abstract).
- Chen, Y.J., Zhai, M.G., and Jiang, S.Y., 2009. Significant achievements and open issues in study of orogenesis and metallogenesis surrounding the North China continent. *Acta Petrologica Sinica*, 25 (11): 2695–2726 (in Chinese with English abstract).
- Cheng, X.H., Xu, J.H., Wang, J.X., Chu, H.X., Xiao, X., and Zhang, H., 2017. Sulfur and Lead isotope constrains on source of ore–forming materials in Asmara VMS–type deposits, Eritrea. *The Chinese Journal of Nonferrous Metals*, 27(4): 795–810 (in Chinese with English abstract).
- Ciobanu, C.L., Cook, N.J., Pring, P., Brugger, J., Danyushevsky, L., and Shimizu, M., 2009. ‘Invisible gold’ in bismuth chalcogenides. *Geochimica et Cosmochimica Acta*, 73: 1970–1999.
- Cook, N.J., Ciobanu, C.L., Pring, A., Skinner, W., Danyushevsky, L., Shimizu, M., Saini–Eidukat, B., and Melcher, F., 2009. Trace and minor elements in sphalerite: A LA–ICP–MS study. *Geochimica et Cosmochimica Acta*, 73: 4761–4791.
- Cook, N.J., Ciobanu, C.L., George, L., Zhu, Z.Y., Wade, B., and Ehrig, K., 2016. Trace element analysis of minerals in magmatic–hydrothermal ores by laser ablation inductively coupled plasma mass spectrometry: Approaches and opportunities. *Minerals*, 6: 111.
- Dare, S.A.S., Barnes, S.J., and Prichard, H.M., 2010. The distribution of platinum group elements and other chalcophile elements among sulfides from the Creighton Ni–Cu–PGE sulfide deposit, Sudbury, Canada, and the origin of Pd in pentlandite. *Mineral Deposita*, 45: 765–793.
- Du, Q.X., Han, Z.R., Shen, X.L., Han, C., Song, Z.G., Gao, L.H., Han, M., Zhong, W.J., and Yan, J.L., 2017. New Evidence of Detrital Zircon Ages for the Final Closure Time of the Paleo–Asian Ocean in the Eastern Central Asian Orogenic Belt (NE China). *Acta Geologica Sinica (English Edition)*, 91(5): 1910–1914.
- Gao, X.S., Wu, W.Q., and Han, S.J., 2010. Geological features and genesis of Dongfengbeishan molybdenum deposit in Tianbaoshan. *Jilin Geology*, 29(4): 43–53 (in Chinese with English abstract).
- George, L.L., Cook, N.J., Crowe, B.B.P., and Ciobanu, C.L., 2018. Trace elements in hydrothermal chalcopyrite. *Mineralogical Magazine*, 82(1), pp: 59–88.
- Gong, H.J., Zhu, L.M., Li, B., Xiong, X., and Ding, L.L., 2017. Geology and Lead–Sulphur Isotope Compositions of the Tongyu Volcanic–Hosted Massive Sulphide Copper Deposit in the Western Part of the North Qinling Orogen, China. *Acta Geologica Sinica (English Edition)*, 91(5): 1767–1777.
- Hu, P., Wu, Y., Zhang, C.Q., and Hu, M.Y., 2014. Trace and minor elements in sphalerite from the Mayuan lead–zinc deposit, northern margin of the Yangtze Plate: Implications from LA–ICP–MS analysis. *Acta Mineralogica Sinica*, 3(4): 461–468 (in Chinese with English abstract).
- Houston, D.L., 1999. Stable isotopes and their significance for understanding the genesis of volcanic–hosted massive sulfide deposits: A review. *Reviews in Economic Geology*, 8: 157–179.
- Jahn, B.M., Wu, F.Y., and Chen, B., 2000. Massive granitoid generation in central Asia: Nd isotopic evidence and implication for continental growth in the Phanerozoic. *Episodes*, 23: 82–92.
- Ju, N., Ren, Y.S., Zhao, H.L., and Wang, H., 2011. Mineralization type and genesis of the Tianbaoshan polymetallic deposit, Yanbian. *Acta Mineralogica Sinica*, 31(Suppl.1): 38–39 (in Chinese).
- Ju, N., 2013. Ore genesis and tectonic settings of Lishan polymetallic deposit in Tianbaoshan metallogenic region, Yanbian area (Master thesis). Changchun: Jilin University, 1–57 (in Chinese with English abstract).
- Kamona, A.F., Leveque, J., and Friedrich, G., 1999. Lead isotopes of the carbonate–hosted Kabwe, Tsumeb, and Kipushi Pb–Zn–Cu sulfide deposits in relation to Pan African orogenesis in the Damaran–Lufilian Fold Belt of Central Africa. *Mineralium Deposita*, 34: 273–283.
- Khain, E.V., Bibikova, E.V., Kröner, A., Zhuravlev, D.Z., Sklyarov, E.V., Fedotova, A.A., and Kravchenko–Bereznoy, I.R., 2002. The most ancient ophiolite of the Central Asian fold belt: U–Pb and Pb–Pb zircon ages for the Dunzhugur Complex, Eastern Sayan, Siberia, and geodynamic implications. *Earth and Planetary Science Letters*, 199: 311–325.
- Kong, Z.G., Wu, Y., Zhang, F., Zhang, C.Q., and Meng, X.Y., 2018. Sources of ore–forming material of typical Pb–Zn deposits in the Sichuan–Yunnan–Guizhou metallogenic province: constraints from the S–Pb isotope compositions. *Earth Science Frontiers*, 25(1): 125–137 (in Chinese with English abstract).
- Leng, C.B., 2017. Genesis of Hongshan Cu polymetallic large deposit in the Zhongdian area, NW Yunnan: constraints from LA–ICPMS trace elements of pyrite and pyrrhotite. *Earth Science Frontiers*, 24(6): 162–175 (in Chinese with English abstract).
- Li, B.S., and Li, H.N., 1991. Polygenesis of Tianbaoshan polymetallic deposit, Jilin province. *Journal of Changchun University of Earth Science*, 21(2): 176–181 (in Chinese with English abstract).
- Liu, J.H., and Song, Q.H., 2000. The ore–forming materials source of the Tianbaoshan–Tianqiaoling polymetallic metallogenic belt in the Yanbian area, Jilin province. *Jilin Geology*, 3: 26–34 (in Chinese with English abstract).
- Liu, S., Hu, R.Z., Gao, S., Feng, C.X., Feng, G.Y., Coulson, I.M., Li, C., Wang, T., and Qi, Y.L., 2010. Zircon U–Pb age and Sr–Nd–Hf isotope geochemistry of Permian granodiorite and associated gabbro in the Songliao Block, NE China and implications for growth of juvenile crust. *Lithos*, 114(3–4): 423–436.
- Liu, W.S., Zhao, R.Y., Zhang, X., Jiang, J.C., Chen, Y.C., Wang, D.H., Ying, L.J., and Liu, Z.Q., 2019. The EPMA and LA–ICP–MS In–situ Geochemical Features of Pyrrhotite and Pyrite in Dabaoshan Cu–polymetallic deposit, North Guangdong Province, and their constraint on genetic mechanism. *Acta Geoscientia Sinica*, 40(2): 291–306 (in Chinese with English abstract).
- Liu, X.D., and Zhou, T.F., 1999. General geological and geochemical characteristics and ore–forming mechanism of the massive sulfide deposits. *Journal of Hefei University of Technology*, 22(4): 45–50 (in Chinese with English abstract).

- Loftus–Hills, G., and Solomon, M., 1967. Cobalt, nickel and selenium in sulfides as indicators of ore genesis. *Mineralium Deposita*, 2(3): 228–242.
- Lu, Y.F., 2004. Geokit: A geochemical toolkit for Microsoft excel. *Geochimica*, 33(5): 459–464 (in Chinese with English abstract).
- Mao, Q.G., Wang, J.B., Fang, T.H., Zhu, J.J., Fu, Y.W., Yu, M.J., and Huang, X.K., 2015. Lead and sulfur isotope studies of sulfides from Honghai VMS–type deposit in Kalatage ore belt of eastern Tianshan Mountains. *Mineral Deposits*, 34(4): 730–744 (in Chinese with English abstract).
- Ohmoto, H., 1972. Systematics of sulfur and carbon isotopes in hydrothermal ore deposits. *Economic Geology*, 67: 551–578.
- Ohmoto, H., and Skinner, B.J., 1983. The Kuroko and related volcanogenic massive sulfide deposit. *Economic Geology*, 5: 604.
- Ohmoto, H., 1986. Stable isotope geochemistry of ore deposits. *Reviews in Mineralogy and Geochemistry*, 16(1): 491–559.
- Ohmoto, H., 1996. Formation of volcanogenic massive sulfide deposits: The Kuruko perspective. *Ore Geology Reviews*, 10: 135–177.
- Ohmoto, H., and Goldhaber, M.B., 1997. Sulfur and carbon isotope. *Geochemistry of Hydrothermal Ore Deposits*, 517–612.
- Ren, Y.S., Ju, N., Chen, C., Yang, Q., Shang, Q.Q., and Lai, K., 2015. Late Paleozoic VMS deposits in eastern Jilin and their tectonic significance. *Acta Mineralogica Sinica*, 35(S1): 493 (in Chinese).
- Sengör, A.M.C., Natalén, B.A., and Burtman, V.S., 1993. Evolution of the Altaid tectonic collage and Paleozoic crustal growth in Eurasia. *Nature*, 364: 299–307.
- Shang, Q.Q., Ren, Y.S., Chen, C., Duan, M.X., Sun, Q., and Xue, S.Y., 2017. Tectonic setting of Guandi iron deposit and Archean crustal growth of Helong Massif in NE China: Evidence from petrogeochemistry, Zircon U–Pb Geochronology and Hf isotope. *Earth Science*, 42(12): 2208–2228 (in Chinese with English abstract).
- Song, G., 1984. Geological characteristics and metallogenic age of breccia pipe Pb–Zn deposit in Tianbaoshan, Jilin Province. *Jilin Geology*, 4: 46–53 (in Chinese).
- Stacey, J.S., and Hedlund, D.C., 1983. Lead–isotope compositions of diverse igneous rocks and ore deposits from southwestern New Mexico and their implications for early Proterozoic crustal evolution in the western United States. *Geological Society of America Bulletin*, 94: 43–57.
- Sun, J., 1994. The characteristics of deposit series and the significance in prospecting in the Tianbaoshan polymetallic deposit, Jilin. *Jilin Geology*, 12 (2): 42–49 (in Chinese with English abstract).
- Sun, J.G., Xing, S.W., Zheng, Q.D., Huang, Y.W., Yin, J.F., Wang, C.F., Li, G.H., Ge, Z.L., and Chen, J.Q., 2006. *Geology and Geochemistry of Nonferrous and Noble Metal Deposit, Northeastern China*. Changchun: Jilin University Press, 1–128 (in Chinese).
- Sun, Z.M., Ren, Y.S., Ju, N., Zhao, H.L., Chen, C., and Sun, Y.C., 2014. Superimposed mineralization of the Tianbaoshan metallogenic region in Yanbian area (eastern Jilin Province), northeastern China: indicated by the isotopic dating. *Acta Petrologica Sinica*, 30(7): 2081–2091 (in Chinese with English abstract).
- Tu, G.C., Gao, Z.M., and Hu, R.Z., 2004. *Geochemistry and Mineralization Mechanism of Dispersed Elements*. Beijing: Geological Publishing House, 1–424 (in Chinese).
- Wang, Z.G., Wang, K.Y., Wan, D., Konare, Y., and Wang, C.Y., 2017a. Genesis of the Tianbaoshan Pb–Zn–Cu–Mo polymetallic deposit in eastern Jilin, NE China: Constraints from fluid inclusions and C–H–O–S–Pb isotope systematics. *Ore Geology Reviews*, 80: 1111–1134.
- Wang, Z.J., 2016. Late Paleozoic–Triassic tectonic evolution of eastern segment of the southern margin of the Xing’an–Mongolia Orogenic Belt: Evidence from detrital zircon U–Pb geochronology and igneous rock associations (Ph.D. thesis). Changchun: Jilin University, 1–145 (in Chinese with English abstract).
- Wang, Z.W., Pei, F.P., Xu, W.L., Cao, H.H., Wang, Z.J., and Zhang, Y., 2016. Tectonic evolution of the eastern Central Asian Orogenic Belt: Evidence from zircon U–Pb–Hf isotopes and geochemistry of early Paleozoic rocks in Yanbian region, NE China. *Gondwana Research*, 38: 334–350.
- Watling, R.J., Herbert, H.K., and Abell, I.D., 1995. The application of laser ablation–inductively coupled plasma–mass spectrometry (LA–ICP–MS) to the analysis of selected sulfide minerals. *Chemical Geology*, 124: 67–81.
- Windley, B.F., Alexeiev, D., Xiao, W.J., Kröner, A., and Badarch, G., 2007. Tectonic model for accretion of the Central Asian Orogenic Belt. *Journal of the Geological Society*, 164: 31–47.
- Wu, F.Y., Zhao, G.C., Sun, D.Y., Wilde, S.A., and Yang, J.H., 2007. The Hulan Group: its role in the evolution of the Central Asian Orogenic Belt of NE China. *Journal of Asian Earth Sciences*, 30: 542–556.
- Wu, F.Y., Sun, D.Y., and Ge, W.C., 2011. Geochronology of the Phanerozoic granitoids in northeastern China. *Journal of Asian Earth Sciences*, 41(1): 1–30.
- Wu, K.X., Hu, R.Z., Bi, X.W., Peng, J.T., and Tang, Q.L., 2002. Ore Lead isotopes as a tracer for ore–forming material sources: A review. *Geology Geochemistry*, 30(3): 73–81 (in Chinese with English abstract).
- Xing, B., Xiang, J.F., Ye, H.T., Chen, X.D., Zhang, G.S., Yang, C.Y., Jin, X., and Hu, Z.Z., 2017. Genesis of Luotuoshan sulfur polymetallic deposit in western Henan Province: Evidence from trace elements of sulfide revealed by using LA–ICP–MS in lamellar ores. *Mineral Deposits*, 36(1): 83–106 (in Chinese with English abstract).
- Xu, W.L., Wang, F., Pei, F.P., Meng, N., Tang, J., Xu, M.J., and Wang, W., 2013. Mesozoic tectonic regimes and regional ore–forming background in NE China: constraints from spatial and temporal variations of Mesozoic volcanic rock associations. *Acta Petrologica Sinica*, 29 (2): 339–353 (in Chinese with English abstract).
- Yang, Q., Ren, Y.S., Ju, N., Zhang, B., Chen, C., and Sun, Z.M., 2015b. Geochronology and geochemistry of the metallogenic intrusion in the Xinxing lead–zinc (silver) deposit in the Tianbaoshan ore concentration area, Yanbian Prefecture. *Acta Petrologica et Mineralogica*, 34(3): 295–308 (in Chinese with English abstract).
- Yang, Q., Ren, Y.S., Sun, Z.M., Hao, Y.J., Zhang, B., Sun, X.H., and Lu, S.Y., 2018. Geochronologic evidence of Late Paleozoic magmatic–hydrothermal mineralization in Tianbaoshan metallogenic region, Yanbian area: A case study of the Xinxing lead–zinc (silver) deposit. *Acta Petrologica Sinica*, 34(10): 3453–3466 (in Chinese with English abstract).
- Ye, L., Cook, N.J., Ciobanu, C.L., Liu, Y.P., Zhang, Q., Liu, T.G., Gao, W., Yang, Y.L., and Danyushevskiy, L., 2011. Trace and minor elements in sphalerite from base metal deposits in South China: A LA–ICPMS study. *Ore Geology Review*, 39: 188–217.
- Ye, L., Gao, W., Yang, Y.L., Liu, T.G., and Peng, S.S., 2012. Trace elements in sphalerite in Laochang Pb–Zn polymetallic deposit, Lancang, Yunnan Province. *Acta Petrologica Sinica*, 28(5): 1362–1372 (in Chinese with English abstract).

- English abstract).
- Zartman, R.E., and Doe, B.R., 1981. Plumbotectonics—the model. *Tectonophysics*, 75: 135–162.
- Zeng, Q.D., Liu, J.M., Qin, K.Z., Fan, H.R., Chu, S.X., Wang, Y.B., and Zhou, L.L., 2013. Types, characteristics, and time–space distribution of molybdenum deposits in China. *International Geology Reviews*, 55: 1311–1358.
- Zhang, M.F., Zhou, Z.G., Xiong, S.F., Gong, Y.J., Chen, G.L., and Li, H., 2016. A typomorphic study of sphalerite from the Huize lead–zinc deposit, Yunnan Province. *Acta Petrologica et Mineralogica*, 35(1): 111–123 (in Chinese with English abstract).
- Zhang, P.F., Li, G.J., Huang, Y.H., Liang, K., Yang, J.B., Liu, Y.C., Mao, F.X., and Zhao, F., 2017. Metallogenic process of Laochang Pb–Zn polymetallic VMS deposit in Sanjiang orogenic belt, SW China: Evidence from fluid inclusion and sulfur isotope. *Acta Petrologica Sinica*, 33(7): 2129–2142 (in Chinese with English abstract).
- Zhang, Q., 1987. Trace elements in galena and sphalerite and their geochemical significance in distinguishing the genetic types of Pb–Zn ore deposits. *Chinese Journal of Geochemistry*, 6: 177–190 (in Chinese).
- Zhang, Y., Sun, J.G., Song, Q.H., Zhao, Z., Chen, D., Men, L.J., Bai, L.A., and Han, S.J., 2011. Ore–forming geological significance and  $^{40}\text{Ar}/^{39}\text{Ar}$  laser probe dating for fluid inclusions in mineral from Tianbaoshan polymetallic deposit, Yanbian. *Journal of Mineralogy and Petrology*, 31(2): 42–47 (in Chinese with English abstract).
- Zhang, Y., Sun, J.G., Chen, D., Xing, S.W., Song, Q.H., Zhao, Z., Zhao, K.Q., Bai, L.A., and Han, S.J., 2012. Characteristics of fluid inclusions and metallogenic model of Tianbaoshan polymetallic ore field, Yanbian, China. *Journal of Jilin University (Earth Science Edition)*, 42(6): 1665–1675 (in Chinese with English abstract).
- Zhang, Y., Sun, J.G., Xing, S.W., Zhao, K.Q., Zang, Z.J., and Ma, Y.B., 2013a. Re–Os dating of molybdenite from Tianbaoshan polymetallic orefield in Yanbian and its geological significance. *Mineral Deposits*, 32(2): 427–435 (in Chinese with English abstract).
- Zhang, Y., Sun, J.G., Chen, Y.J., and Zhao, K.Q., 2013b. Re–Os and U–Pb geochronology of porphyry Mo deposits in central Jilin Province: Mo ore–forming stages in northeast China. *International Geology Reviews*, 14: 1763–1785.
- Zhang, Y.B., Wu, F.Y., Wilde, S.A., Zhai, M.G., Lu, X.P., and Sun, D.Y., 2004. Zircon U–Pb ages and tectonic implications of ‘Early Paleozoic’ granitoids at Yanbian, Jilin Province, northeast China. *The Island Arc*, 13: 484–505.
- Zhao, X., 2018. Geological characteristics and metallogenic model of Shijing gold–silver deposit in Yanbian area (Master thesis). Changchun: Jilin University, 1–60 (in Chinese with English abstract).

#### About the first author

LU Siyu, male, born in 1995 in Tonghua City, Jilin Province; master; graduated from College of Earth Sciences, Jilin University. He is now interested in the study on VMS deposit, mineral resource prospecting and exploration in NE China. E–mail: lusy18@mails.jlu.edu.cn; phone: 15754300558.



#### About the corresponding author

REN Yunsheng, male, born in 1969 in Tangshan City, Hebei Province; professor; graduated from College of Earth Sciences, Jilin University. He is now interested in the study on hydrothermal deposit, mineral resource prospecting and exploration. E–mail: renyuns@jlu.edu.cn; phone: 0431–88502708, 13154370506.

